ARTICLE

doi:10.1038/nature18632

Multiple mechanisms disrupt the *let-7* microRNA family in neuroblastoma

John T. Powers[1], Kaloyan M. Tsanov[1], Daniel S. Pearson[1], Frederik Roels[2], Catherine S. Spina[3], Richard Ebright[1], Marc Seligson[1], Yvanka de Soysa[1], Patrick Cahan[1], Jessica Theißen[2], Ho-Chou Tu[1], Areum Han[1], Kyle C. Kurek[4], Grace S. LaPier[1], Jihan K. Osborne[1], Samantha J. Ross[1], Marcella Cesana[1], James J. Collins[3,5], Frank Berthold[2] & George Q. Daley[1,6,7,8]

Poor prognosis in neuroblastoma is associated with genetic amplification of *MYCN*. *MYCN* is itself a target of *let-7*, a tumour suppressor family of microRNAs implicated in numerous cancers. *LIN28B*, an inhibitor of *let-7* biogenesis, is overexpressed in neuroblastoma and has been reported to regulate *MYCN*. Here we show, however, that *LIN28B* is dispensable in *MYCN*-amplified neuroblastoma cell lines, despite de-repression of *let-7*. We further demonstrate that *MYCN* messenger RNA levels in amplified disease are exceptionally high and sufficient to sponge *let-7*, which reconciles the dispensability of *LIN28B*. We found that genetic loss of *let-7* is common in neuroblastoma, inversely associated with *MYCN* amplification, and independently associated with poor outcomes, providing a rationale for chromosomal loss patterns in neuroblastoma. We propose that *let-7* disruption by *LIN28B*, *MYCN* sponging, or genetic loss is a unifying mechanism of neuroblastoma development with broad implications for cancer pathogenesis.

Carcinogenesis involves multiple genetic and epigenetic events, yet the organizing principles underlying their choreography are poorly understood. MicroRNA (miRNA) deregulation is an important component of this landscape through both oncogenic and tumour-suppressive functions of miRNAs[1]. Of these, the highly conserved *let-7* family has a prominent role in the regulation of embryonic development and maintenance of differentiated tissues and is among the most abundantly expressed miRNAs. It serves as a potent tumour suppressor via post-transcriptional repression of multiple oncogenic messenger RNA (mRNA) targets including *RAS*, *MYC*, and *HMGA2* (refs 2–4). The *let-7* family is downregulated in multiple tumour types and has been causally linked to oncogenesis[1,5–8]. Uncovering the mechanisms by which *let-7* function is neutralized is therefore critical to both the fundamental understanding of cancer pathogenesis and novel therapies.

Several mechanisms of *let-7* disruption have emerged in different contexts. First, its biogenesis can be suppressed by the *LIN28B* RNA-binding protein[9], a highly conserved heterochronic gene implicated in cancer and reported to induce tumours in multiple mouse models including hepatocellular carcinoma, colon cancer, Wilms tumour, and neuroblastoma[10–16]. Second, competing endogenous RNAs (ceRNAs) have been proposed to sponge miRNAs, including *let-7*, diluting their activity through competition for miRNAs with sites common to multiple ceRNA species[17–19]. Third, chromosome loss is a suggested mechanism of *let-7* disruption in cancer, as genetic deletion of *let-7* is associated with several solid tumours[1].

The neuroblastoma master oncogene, *MYCN*, has a 910-nucleotide-long 3′ untranslated region (UTR) containing two *let-7* binding sites which are almost perfectly conserved among land vertebrates, suggesting strong functional relevance[20–22] (Extended Data Fig. 1). Coding sequence mutations in neuroblastoma are rare[23,24], whereas chromosome arm gain or loss events are common[25,26]. The most well-known chromosomal aberration is amplification of the *MYCN* locus, which occurs in ~25% of all neuroblastomas and largely defines poor prognosis[27,28]. Other common chromosomal deletions at chromosome arms 3p and 11q are inversely associated with *MYCN* amplification. The reason for this discordance is unknown.

Here we set out to understand the relationship between *MYCN* and *let-7* in neuroblastoma. A complex relationship emerges between *LIN28B* activity, a novel ceRNA function of the *MYCN* 3′ UTR, and *let-7* genetic loss, which together present a unifying model of *let-7* suppression during neuroblastoma pathogenesis. This model provides an organizing principle for understanding distinct genetic patterning in neuroblastoma, with potential implications for cancer in general.

LIN28B and *let-7* regulate the *MYCN* 3′ UTR

LIN28B is highly expressed in human neuroblastoma and its expression correlates with tumour stage, rendering the *LIN28B*/*let-7* axis an attractive target for interrogation (Extended Data Fig. 2a–d). Two recent reports concluded that this pathway plays a critical role in regulating *MYCN* and neuroblastoma cell growth[12,13]. To examine the relationship between the *MYCN* transcript, *let-7* and *LIN28B*, we first transfected non-*MYCN* amplified neuroblastoma cells with the *MYCN* open reading frame (ORF), with or without the 3′ UTR carrying intact or mutant *let-7* sites (Fig. 1a). The full-length wild-type *MYCN* transcript produced markedly lower MYCN protein levels than the ORF-only construct. Mutation of the *let-7* sites in the 3′ UTR partly rescued MYCN expression, implicating *let-7* modulation as an important component of *MYCN* post-transcriptional regulation (Fig. 1b). Expression of *LIN28B* suppressed the *let-7* family in non-*MYCN*-amplified neuroblastoma cells and conferred a growth advantage. *LIN28B* rescued expression of the wild-type 3′ UTR construct, demonstrating that *LIN28B* can support *MYCN* expression through *let-7* repression in the absence of *MYCN* amplification (Extended Data Fig. 2e, f and Fig. 1c). However, when we transfected *MYCN*-amplified cells with a *let-7a* mimic, we observed decreased MYCN protein levels only above 15- and 80-fold increases in cellular levels of *let-7a*, respectively,

[1]Division of Pediatric Hematology/Oncology, Boston Children's Hospital, Boston, Massachusetts 02115, USA. [2]Department of Pediatric Oncology, University Hospital Köln, Köln 50937, Germany. [3]Wyss Institute for Biologically Inspired Engineering, Boston, Massachusetts 02115, USA. [4]Department of Pathology, Boston Children's Hospital, Boston Massachusetts 02215, USA. [5]Department of Biological Engineering, Massachusetts Institute of Technology, Broad Institute of MIT and Harvard, Cambridge, Massachusetts 02142, USA. [6]Stem Cell Transplantation Program, Dana Farber Cancer Institute & Boston Children's Hospital, Boston, Massachusetts 02115, USA. [7]Department of Biological Chemistry & Molecular Pharmacology, Harvard Medical School, Boston, Massachusetts 02115, USA. [8]Harvard Stem Cell Institute, Cambridge, Massachusetts 02138, USA.

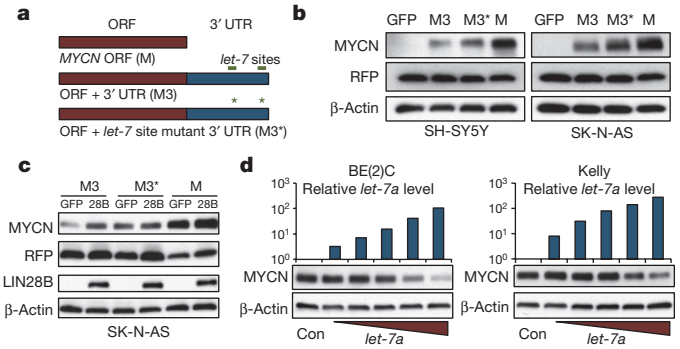

Figure 1 | The *LIN28B*/*let-7*/*MYCN* axis is intact in neuroblastoma. **a**, pcDNA3.1:*MYCN* constructs. **b**, Immunoblot for indicated proteins in non-*MYCN*-amplified neuroblastoma cells transfected with indicated constructs. **c**, Immunoblot for indicated proteins in green fluorescent protein (*GFP*)- or *LIN28B*-expressing cells transfected as in **b**. **d**, qPCR analysis of *let-7a* levels and immunoblot for MYCN in *MYCN*-amplified cells transfected with control or *let-7a* mimic dose curve (data representative of three independent experiments). For gel source data, see Supplementary Figures.

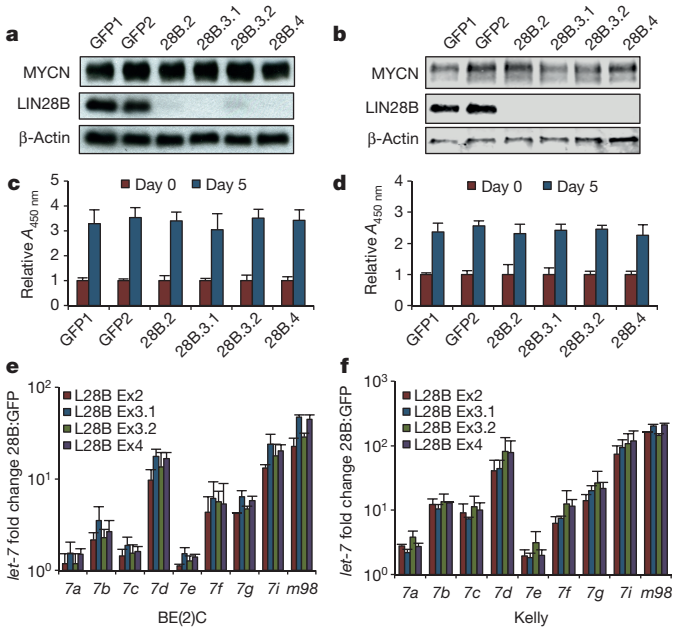

Figure 2 | *LIN28B* is dispensable in human *MYCN* amplified neuroblastoma cells. a, **b**, Immunoblot for MYCN and LIN28B in cells infected with indicated Cas9-gRNA lentivirus. For gel source data, see Supplementary Figures. **c**, **d**, Cell growth analysis of cells infected as in **a**, **b** (BrdU incorporation; relative absorbance, *A*, at 450 nm). **e**, **f**, qPCR analysis of relative *let-7* expression in cells from **a** and **b** respectively. Fold change relative to GFP gRNA controls ($n = 3$ independent experiments, mean + s.e.m. shown).

suggesting that *MYCN* was refractory to all but exceedingly high levels of exogenous *let-7* (Fig. 1d).

LIN28B is dispensable in *MYCN*-amplified cells

Next, we evaluated the previously reported *LIN28B-let-7-MYCN* regulatory circuit using published lentiviral short hairpin RNA (shRNA) constructs to knockdown *LIN28B* in *MYCN*-amplified neuroblastoma cells and observed comparable suppression of MYCN protein levels and cell growth (Extended Data Fig. 3a, b). We further observed reduced xenograft tumour growth in cells expressing a *LIN28B* targeting shRNA (Extended Data Fig. 3c). However, we did not observe an appreciable de-repression of *let-7* levels upon shRNA-mediated *LIN28B* knockdown, which is counter to the established model (Extended Data Fig. 3d). Moreover, we were unable to rescue these effects through overexpression of shRNA-resistant *LIN28B* constructs (Extended Data Fig. 3e, f). Together, these data suggest that the reported effects of the shRNAs on both cell growth and MYCN protein levels might be due to hairpin-induced toxicities.

As an alternative approach to depleting *LIN28B*, we tested five small interfering RNAs (siRNAs) and found that four both effectively knocked down *LIN28B* and, as expected, de-repressed *let-7* levels (Extended Data Fig. 4a–d). Upon extended serial siRNA transfection, we observed that despite robust *LIN28B* knockdown and strong de-repression of *let-7*, MYCN protein levels were unaffected and there was no appreciable effect on cell proliferation (Extended Data Fig. 4e–g).

To exclude the possibility of incomplete knockdown resulting in residual *LIN28B* activity, we employed *Cas9* and four distinct guide RNAs (gRNAs) targeting *LIN28B* (Extended Data Fig. 4h). We observed robust loss of LIN28B protein with all four gRNA constructs (Fig. 2a, b), indicating efficient disruption of the locus. We did not observe appreciable loss of MYCN protein expression or impaired cell growth, thus corroborating our siRNA-based results (Fig. 2a–d). In addition, the *let-7* family was robustly de-repressed, consistent with the existing *LIN28B/let-7* model (Fig. 2e, f). These observations indicate that disruption of *LIN28B* has little net impact on *MYCN*-amplified neuroblastoma cells.

Amplified *MYCN* mRNA is a *let-7* sponge

The persistence of MYCN protein levels despite high levels of transfected *let-7a* or robust de-repression of *let-7* upon *LIN28B* loss prompted us to explore novel mechanisms of *let-7* perturbation. We hypothesized that there might be a ceRNA in *MYCN*-amplified neuroblastoma cells that serves to sponge *let-7*. To identify potential ceRNAs, we performed poly-A selected RNA-sequencing (mRNA-seq) on *MYCN*-amplified (BE(2)C and Kelly) and non-*MYCN*-amplified (SH-SY5Y) cells. We then determined the relative contribution of *let-7* target sites provided by expressed *let-7* targets. Interestingly, *MYCN* itself was by far the most abundant *let-7* target mRNA in both BE(2)C and Kelly cells, alone providing 19.3% and 18.5% of the entire cellular *let-7* target-site pool, respectively. In contrast, *MYCN* represented only 0.15% of the *let-7* target-site pool in SH-SY5Y cells (Fig. 3a). In fact, *MYCN* mRNA was the second highest expressed mRNA in both BE(2)C and Kelly cells as opposed to the 5,409th highest in SH-SY5Y, demonstrating an exceptionally high *MYCN* mRNA level in *MYCN*-amplified cells (>100-fold increase; Fig. 3b). Other multiple-*let-7*-site mRNAs such as *HMGA2*, *IMP1*, and *ARID3B* were expressed at much lower levels, together suggesting that *MYCN* mRNA might itself be the sponge (Extended Data Fig. 5a). This expression pattern was validated by quantitative PCR (qPCR) in a panel of additional cell lines (Extended Data Fig. 5b).

ceRNA relationships were initially defined in part by similar expression levels between RNAs with similar 3′ UTRs[18,29]. Two recent reports have refined this original precept, suggesting that for a given miRNA family, the miRNA:mRNA-target ratio is a major determinant of how effectively a ceRNA can impact the function of a miRNA family. At low ratios, miRNAs are sensitive to moderate levels of ceRNAs, whereas highly expressed miRNAs with high ratios are difficult to sponge, requiring very high levels of ceRNA[30,31]. We therefore assessed total copies per cell of both *MYCN* mRNA and the *let-7* family in BE(2)C and Kelly cells through quantified mRNA-seq and small-RNA sequencing (sRNA-seq) (Extended Data Fig. 6).

We calculated 13,255 and 10,615 *MYCN* mRNA copies per BE(2)C and Kelly cell, respectively, resulting in 26,511 and 21,231 *let-7* target sites provided by *MYCN* (Fig. 3c top). In stark contrast, there were only 31 *MYCN* transcripts per SH-SY5Y cell. Quantification of the *let-7* family in BE(2)C and Kelly cells yielded 7,259 and 1,952 total *let-7* molecules per cell (Fig. 3c bottom), and *MYCN-let-7*-site:*let-7* miRNA ratios of 3.65 and 10.88, respectively. These ratios satisfy the tenets of the ratio-based ceRNA model and do so as the result of a single

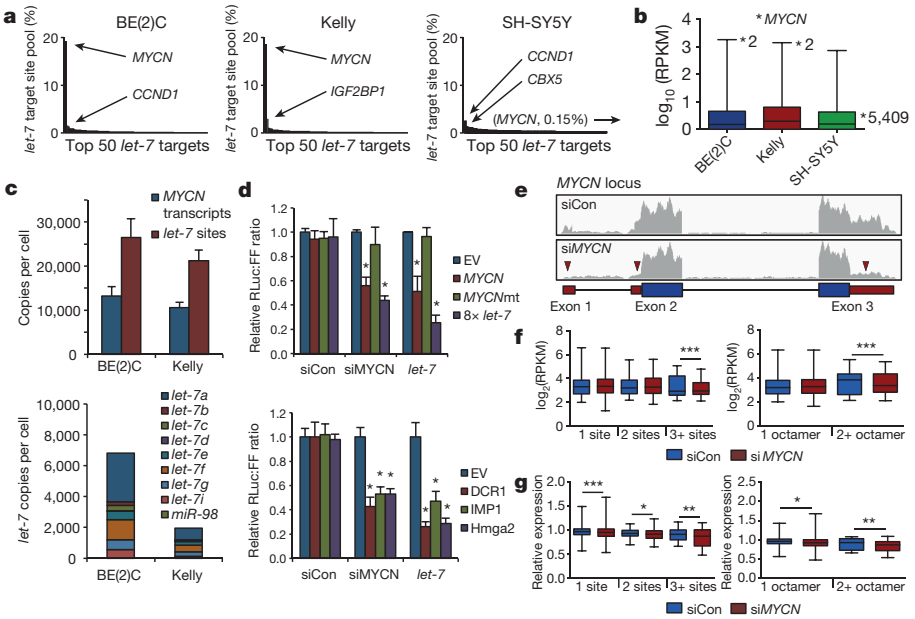

Figure 3 | *MYCN* mRNA is a ceRNA for *let-7*. **a**, The *let-7* target-site pool contribution of the top 50 targets. Arrows indicate top two contributors ($n = 3$ biological replicates, Gene Expression Omnibus accession number GSE81498, see Source Data F3 in Supplementary Information). **b**, Box and whisker plot of top 14,000 expressed mRNAs from data set described in **a**. *MYCN* expression rank marked by asterisk (GSE81498, see Source Data F3). **c**, Top: *MYCN* transcripts and *let-7* sites provided per cell as determined by the data set from **a** (mean + s.d. shown, GSE81498, see Source Data F3). Bottom: *let-7* copies per cell as determined by sRNA-seq ($n = 3$ biological replicates, GSE81499, see Source Data F3). **d**, Top: relative fluorescence ratio in BE(2)C cells co-transfected with indicated constructs small RNAs. Bottom: relative fluorescence ratio in cells co-transfected with indicated constructs and small RNAs. Mean of four independent experiments plus s.e.m. ($*P < 0.05$ relative to empty vector, unpaired *t*-test). **e**, mRNA-seq reads mapping to the *MYCN* locus in BE(2)C:MYCN cells transfected with indicated siRNAs. Blue and red boxes indicate *MYCN* ORFs and UTRs, respectively. Triangles mark reduction of *MYCN* mRNA UTRs. **f**, Expression levels of mRNAs with one, two, or three or more *let-7* sites (left) or with one or two or more octamer *let-7* sites (right) in siCon and si*MYCN* cells (data represent one round of mRNA-seq, $***P < 0.0001$, one-tailed Wilcoxon test). **g**, Relative expression of mRNAs with one, two, or three or more *let-7* sites (left) or with one or two or more octamer *let-7* sites (right) in siCon and si*MYCN* cells co-transfected with *let-7a*. Values relative to miRCon. (Data represent one round of mRNA-seq, $*P < 0.05$, $**P < 0.001$, $***P < 0.001$ versus siCon, one-tailed Wilcoxon test, GSE81497, see Source Data F3).

amplified mRNA. Interestingly, *let-7a* was the most highly expressed *let-7* family member in both cell types, accounting for over half of all *let-7* molecules. These observations were confirmed by spike-in qPCR-based quantification of both *MYCN* and *let-7* (Extended Data Fig. 7a, b). Even upon *LIN28B* knockout, the *MYCN*-*let-7*-site:*let-7* ratio is 1.35 in BE(2)C and 1.78 in Kelly, which remain favourable for ceRNA activity (Extended Data Fig. 7c).

To test the capacity of *MYCN* mRNA to serve as a *let-7* sponge, we co-transfected BE(2)C cells with a series of luciferase constructs containing the 3′ UTRs of several representative *let-7* targets and control or *MYCN* ORF targeting siRNA (Extended Data Fig. 8a, b). Luciferase ratios of all constructs except for empty vector controls and the *let-7*-site-mutated *MYCN*-3′ UTR were significantly reduced by either *MYCN* knockdown or *let-7a* transfection (Fig. 3d), suggesting that the endogenous *MYCN*-3′ UTR sponges steady-state levels of *let-7*. We then tested the sufficiency of the *MYCN*-3′ UTR to de-repress *let-7* targets through sponging of a *let-7a* mimic. We co-transfected the above luciferase reporter constructs with chimaeric *RFP*:*MYCN*-3′ UTR constructs and assayed luciferase activity (Extended Data Fig. 8c, d). The *let-7* target constructs were rescued when co-transfected with wild-type but not *let-7*-site-mutant *MYCN*-3′ UTR (Extended Data Fig. 8e). In addition, exogenous *MYCN*-3′ UTR was sufficient to enhance MYCN protein expression itself in SK-N-AS cells (Extended Data Fig. 8f).

We next tested whether endogenous *let-7* targets are similarly affected. Upon *MYCN* knockdown, protein levels of DICER1, HK2, IMP1, and LIN28B were reduced, while neither mRNA nor *let-7* levels were significantly changed (Extended Data Fig. 9a–c). Concurrent *let-7* inhibition rescued expression of the four targets, supporting post-transcriptional suppression through *let-7* upon *MYCN* knockdown that is consistent with *MYCN* mRNA serving as a *let-7* sponge (Extended Data Fig. 9a). Further, these targets were not reduced at the protein level upon *LIN28B* knockout, which is consistent with this model (Extended Data Fig. 9d).

Lastly, we analysed global *let-7* target expression in response to depletion of the endogenous *MYCN* 3′ UTR. To specifically assess the role of the 3′ UTR, we transfected BE(2)C cells expressing a *MYCN* ORF transgene with a *MYCN* 3′ UTR-targeting siRNA (Fig. 3e). Although we did not see a global reduction of *let-7* targets as a whole (Extended Data Fig. 9e), we did observe significantly lower expression of *let-7* targets with three or more total sites or more than one octamer *let-7* site in their 3′ UTRs, which together define the most sensitive *let-7* targets[32,33] (Fig. 3f). Given the regulation of the *MYCN* 3′ UTR by multiple miRNAs[34] and unknown kinetics of how *let-7* activity is restored after the removal of a ceRNA, we further challenged siCon and si*MYCN* cells with a modest amount of *let-7a* mimic, increasing cellular *let-7* levels approximately eightfold (Extended Data Fig. 9f). We then observed significantly reduced expression across all categories of *let-7* targets in si*MYCN* cells, consistent with increased sensitivity to *let-7* in the absence of the *MYCN* 3′ UTR (Fig. 3g and Extended Data Fig. 9g).

Chromosomal loss of *let-7* in neuroblastoma

While neuroblastoma has a low mutation rate, chromosome arm gain and loss is frequent[23,24]. Two of the most common chromosomal losses in neuroblastoma, chromosome arm 3p (Chr3p, ~33% incidence) and Chr11q (~45% incidence), often occur together and seldom with *MYCN* amplification[23,35,36] (Fig. 4a and Extended Data Fig. 10). Upon analysis of Chr3p and Chr11q, we noted that the Chr3p-loss smallest region of overlap spans from 3p25.3 to 3p14.3 (ref. 37), placing *let-7g*

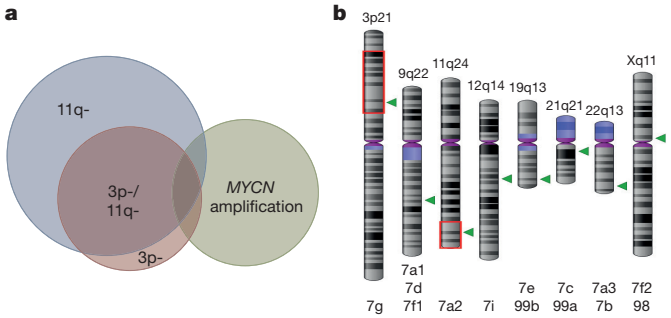

Figure 4 | Loss of *let-7a2* and *let-7g* is common in neuroblastoma. **a**, Scaled Venn diagram assembled from ref. 23 detailing relative incidence and intersection of chromosome 11q and 3p loss and *MYCN* amplification. **b**, Genetic locations of 12 distinct *let-7* family members. Green triangles, *let-7* loci. Red boxes indicate the smallest region of overlap for these deletions. (Images created at http://www.ncbi.nlm.nih.gov/genome/tools/gdp/.)

within the smallest region of overlap and resulting in its loss whenever Chr3p is lost. In addition, the most common breakpoint of Chr11q immediately proximal to the *let-7a2* locus, resulting in loss of *let-7a2* in virtually all Chr11q deletions[35] (Fig. 4b). Moreover, loss of Chr11q in neuroblastoma results in lower overall *let-7a* levels despite loss of only one of three distinct *let-7a* loci[38]. These observations suggest that *let-7* genetic disruption may be selected for in neuroblastoma.

A model in which amplified *MYCN* sequesters mature *let-7* would predict that selective pressure to genetically lose *let-7* might be relieved in *MYCN*-amplified disease. Chr3p (*let-7g*) and Chr11q (*let-7a2*) loss patterns are indeed consistent with such a model. To investigate whether the extended *let-7* family (Fig. 4b) follows this loss pattern, we expanded our analysis to all eight *let-7* genetic loci in 202 neuroblastomas by array comparative genomic hybridization (aCGH). We created a heat-map of copy number estimates for each miRNA locus to compare *MYCN*-amplified with non-amplified copy number values and observed a significant difference for six *let-7* loci (Fig. 5a, b top). At least one *let-7* family member was lost in 63.4% of non-amplified tumours and in only 16.7% of amplified (Fig. 5b top), resulting in average *let-7* copy number changes of −1.94 and −0.36 per tumour, respectively (Fig. 5b bottom). This pattern of copy number loss for *let-7* is distinct from the unrelated *miR-103a* family (Fig. 5b), suggesting that the *let-7* pattern is not reflective of general chromosomal patterning.

The most commonly lost were *let-7a2*, *let-7f2*, and *let-7g*, whereas *let-7a3/7b* and *let-7i* were not significantly lost in any tumour subset. We reasoned that loss frequency might relate to initial expression level. To interrogate this possibility, we used publicly available sRNA-seq data to examine the relative expression levels of mature *let-7* in 12 distinct primary and tumour cell lines that have intact *let-7* loci (Extended Data Fig. 10b). We observed that *let-7a*, *let-7f*, and *let-7g* are present at higher relative levels than other *let-7* family members, which mirrors the copy number loss patterns in non-*MYCN*-amplified neuroblastoma (Fig. 5c). *MiR-100*, the miRNA-cluster partner of *let-7a2*, is more highly expressed than most *let-7s* and their cluster partners, suggesting that

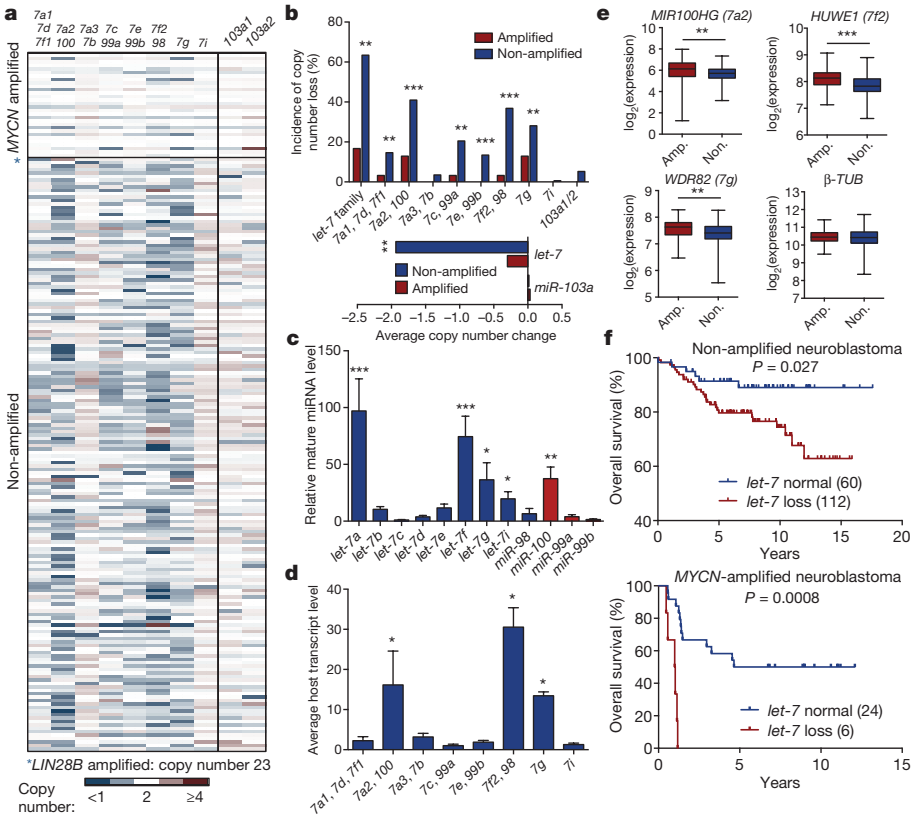

Figure 5 | The *MYCN* aceRNA model predicts *let-7* chromosomal loss patterns in neuroblastoma. **a**, The *let-7* and *miR-103a* loci copy number heat-map based on aCGH relative fluorescence ratios of tumour versus germline (Source Data F5 in Supplementary Information). **b**, Copy number loss incidence for *let-7* and *miR-103a* from data set in **a** (top). Average copy number change for the two miRNA families (bottom). (*$P<0.05$, **$P<0.01$, ***$P<0.001$ amplified versus non-amplified for each locus, unpaired *t*-test, Source Data F5.) **c**, Mature *let-7* expression based on ENCODE sRNA-seq data. (*$P<0.05$, **$P<0.01$, ***$P<0.001$ versus *let-7c*, Wilcoxon test, Source Data F5.) **d**, Relative *let-7* host transcript levels based on ENCODE mRNA-seq data. (*$P<0.05$, **$P<0.01$ versus *let-7c*, Wilcoxon test, Source Data F3.) **e**, Relative expression of indicated host genes in *MYCN*-amplified (Amp.) and non-amplified (Non.) neuroblastoma. *β-TUB* shown as control ($n=498$, **$P<0.01$, ***$P<0.001$, unpaired *t-test*, Source Data F5). **f**, Overall survival curves of neuroblastoma patients in non-amplified (top), and *MYCN*-amplified (bottom) neuroblastoma. *P* values determined by Mantel–Cox test (Source Data F5).

the bulk of the *let-7a* reads may come from the *let-7a2*/*miR-100* locus (Fig. 5c).

A limitation of sRNA-seq is that it cannot distinguish between loci that produce the same mature miRNA. Family members of *let-7* are coordinately transcribed as part of larger host transcripts from which they are then processed, which allows for locus-specific expression analysis[7,39,40] (Extended Data Fig. 10c). We therefore analysed relative expression levels of *let-7* host transcripts in six primary and tumour cell lines. Host transcript levels for *let-7a2*, *let-7f2*, and *let-7g* were significantly higher than for other *let-7* host transcripts (Extended Data Fig. 10d and Fig. 5d), reflecting the pattern of most frequent locus loss in non-amplified disease. In addition, analysis of existing human neuroblastoma mRNA-seq and microarray data sets revealed lower expression of the *let-7a2*, *let-7f2*, and *let-7g* host transcripts in non-amplified compared with *MYCN*-amplified tumours, which is consistent with observed patterns of copy number loss in our aCGH data set (Fig. 5e and Extended Data Fig. 10e). Further, *MYCN* and *let-7* expression are negatively correlated in non-amplified disease, underscoring the importance of *let-7* disruption in the absence of the *MYCN* ceRNA[34]. These data may collectively explain both preferential loss of certain *let-7* loci and common patterns of chromosomal loss in neuroblastoma.

Further emphasizing the significance of *let-7* suppression is the observation that non-*MYCN*-amplified neuroblastoma patients had significantly worse overall survival if there was a *let-7* copy number loss event (Fig. 5f top). In the rare case where *MYCN* amplification and *let-7* copy number loss occurred together, overall survival was dramatically reduced relative to the already-poor prognosis of *MYCN* amplification (Fig. 5f bottom), suggesting a deleterious synergy between two powerful but typically exclusive mechanisms of functional *let-7* disruption.

Of note, one of the tumours in the aCGH data set had genetic amplification of *LIN28B* (copy number = 23; Fig. 5a). This tumour patterned closely with *MYCN*-amplified tumours with regard to net *let-7* loss and tumour stage (IV) despite being 2*n* for *MYCN*. This may represent a case where *LIN28B* significantly contributed to neuroblastoma through *let-7* suppression, similar to the reported mouse model of murine-*Lin28b* driven neuroblastoma[12].

Discussion

The known functionality of *LIN28B*, together with the patterns of genetic deletion of *let-7* and amplified *MYCN* ceRNA (aceRNA) activity described here, establish that neuroblastoma employs multiple mechanisms to neutralize *let-7*, placing *let-7* disruption at the centre of neuroblastoma pathogenesis. We thus propose that *let-7* biogenesis and function are targeted in neuroblastoma by several disparate mechanisms: high frequency genetic loss, *LIN28B* activity, or *MYCN* aceRNA (Extended Data Fig. 10f). This model has implications for our understanding of neuroblastoma pathogenesis, disease modelling, and the rational design of therapeutic strategies, and may represent a more general feature of human cancer.

First, our model offers a plausible explanation for the uniquely high *MYCN* mRNA levels in amplified neuroblastoma, which enable both robust expression of MYCN protein and adequate copies of a ceRNA sufficient to impair the function of a highly expressed miRNA such as *let-7*. Questions may remain about whether an observed >100-fold increase in *MYCN* mRNA, which increases the total *let-7* target sites across the cellular pool of mRNAs by only approximately 25%, is sufficient to mediate a ceRNA effect on *let-7*. However, our functional data based on loss of the *MYCN* 3′ UTR, including candidate reporter analysis of *let-7*-site-containing 3′ UTRs and global *let-7*-target mRNA-seq analysis (Fig. 3d–g), suggest that *MYCN* mRNA may be a preferred target that in abundance can sequester and impair *let-7*. Further, in tumours lacking *MYCN* amplification, our model suggests that selective pressure to disrupt *let-7* explains the well-known, yet unresolved, patterns of *MYCN*-amplification-independent chromosome 3p and 11q loss. AceRNA function of *MYCN* mRNA also accounts for the dispensability of *LIN28B* in *MYCN*-amplified cell lines, suggesting that *LIN28B* may serve a redundant *let-7* suppressive role.

Our findings suggest that highly expressed 3′ UTRs contribute to miRNA deregulation in cancer, and therefore both coding and non-coding functions of oncogenic mRNAs should be considered in animal tumour modelling. For example, both the TH-*MYCN* and LSL-*MYCN;Dbh-iCre* models of murine neuroblastoma overexpress the *MYCN* ORF and lack 3′ UTRs. Notably, the TH-*MYCN* model has similar patterns of *let-7a2*, *let-7f2*, and *let-7g* genetic loss as non-amplified human disease and both models broadly downregulate the *let-7* family[34,41], further suggesting that *let-7* disruption is important even in the presence of *MYCN* protein expression. Moreover, a recent report demonstrates that high-level expression of the *BRAF* pseudogene, which contains a functional 3′ UTR but does not encode a protein, is sufficient to induce lymphoma in mice[42]. Consequently, full-length mRNA transgenes may yield more accurate genetic modelling of human tumours in animals.

Lastly, our model establishes *let-7* restoration as a key therapeutic goal in neuroblastoma. There are few neuroblastoma-specific therapies, and attempts to directly target *MYCN* have met with little success, despite efforts spanning the past 20 years (refs 25, 26, 43). The fact that *MYCN* mRNA has such a strong functional connection to *let-7* exposes a valuable opportunity to target *MYCN* itself and provides hope of delivering disease-specific therapy to the worst prognostic class of neuroblastoma.

We show here that disparate modes of *let-7* suppression are selectively and inversely related in neuroblastoma. Given that both oncogenic amplification and disruption of *let-7* biogenesis appear to play central roles in multiple cancer types[15,44–47], our model may provide a novel organizing principle by which to consider and interrogate genetic events in a broad range of tumours.

Online Content Methods, along with any additional Extended Data display items and Source Data, are available in the online version of the paper; references unique to these sections appear only in the online paper.

Received 2 February 2015; accepted 8 June 2016.
Published online 6 July 2016.

1. Croce, C. M. Causes and consequences of microRNA dysregulation in cancer. *Nature Rev. Genet.* **10,** 704–714 (2009).
2. Johnson, S. M. *et al.* RAS is regulated by the let-7 microRNA family. *Cell* **120,** 635–647 (2005).
3. Sampson, V. B. *et al.* MicroRNA let-7a down-regulates MYC and reverts MYC-induced growth in Burkitt lymphoma cells. *Cancer Res.* **67,** 9762–9770 (2007).
4. Mayr, C., Hemann, M. T. & Bartel, D. P. Disrupting the pairing between let-7 and Hmga2 enhances oncogenic transformation. *Science* **315,** 1576–1579 (2007).
5. Lu, J. *et al.* MicroRNA expression profiles classify human cancers. *Nature* **435,** 834–838 (2005).
6. Boyerinas, B., Park, S.-M., Hau, A., Murmann, A. E. & Peter, M. E. The role of let-7 in cell differentiation and cancer. *Endocr. Relat. Cancer* **17,** F19–F36 (2010).
7. Gurtan, A. M. & Sharp, P. A. The role of miRNAs in regulating gene expression networks. *J. Mol. Biol.* **425,** 3582–3600 (2013).
8. Blandino, G. *et al.* Tumor suppressor microRNAs: a novel non-coding alliance against cancer. *FEBS Lett.* **588,** 2639–2652 (2014).
9. Viswanathan, S. R., Daley, G. Q. & Gregory, R. I. Selective blockade of microRNA processing by Lin28. *Science* **320,** 97–100 (2008).
10. Nguyen, L. H. *et al.* Lin28b is sufficient to drive liver cancer and necessary for its maintenance in murine models. *Cancer Cell* **26,** 248–261 (2014).
11. Viswanathan, S. R. *et al.* Lin28 promotes transformation and is associated with advanced human malignancies. *Nature Genet.* **41,** 843–848 (2009).
12. Molenaar, J. J. *et al.* LIN28B induces neuroblastoma and enhances MYCN levels via *let-7* suppression. *Nature Genet.* **44,** 1199–1206 (2012).
13. Diskin, S. J. *et al.* Common variation at 6q16 within *HACE1* and *LIN28B* influences susceptibility to neuroblastoma. *Nature Genet.* **44,** 1126–1130 (2012).
14. Madison, B. B. *et al.* LIN28B promotes growth and tumorigenesis of the intestinal epithelium via Let-7. *Genes Dev.* **27,** 2233–2245 (2013).
15. Urbach, A. *et al.* Lin28 sustains early renal progenitors and induces Wilms tumor. *Genes Dev.* **28,** 971–982 (2014).
16. Tu, H. C. *et al.* LIN28 cooperates with WNT signaling to drive invasive intestinal and colorectal adenocarcinoma in mice and humans. *Genes Dev.* **29,** 1074–1086 (2015).

17. Tay, Y., Rinn, J. & Pandolfi, P. P. The multilayered complexity of ceRNA crosstalk and competition. *Nature* **505,** 344–352 (2014).
18. Poliseno, L. *et al.* A coding-independent function of gene and pseudogene mRNAs regulates tumour biology. *Nature* **465,** 1033–1038 (2010).
19. Cesana, M. & Daley, G. Q. Deciphering the rules of ceRNA networks. *Proc. Natl Acad. Sci. USA* **110,** 7112–7113 (2013).
20. Lewis, B. P., Burge, C. B. & Bartel, D. P. Conserved seed pairing, often flanked by adenosines, indicates that thousands of human genes are microRNA targets. *Cell* **120,** 15–20 (2005).
21. Melton, C., Judson, R. L. & Blelloch, R. Opposing microRNA families regulate self-renewal in mouse embryonic stem cells. *Nature* **463,** 621–626 (2010).
22. Baeyens, K. J., De Bondt, H. L., Pardi, A. & Holbrook, S. R. A curved RNA helix incorporating an internal loop with G·A and A·A non-Watson–Crick base pairing. *Proc. Natl Acad. Sci. USA* **93,** 12851–12855 (1996).
23. Pugh, T. J. *et al.* The genetic landscape of high-risk neuroblastoma. *Nature Genet.* **45,** 279–284 (2013).
24. Molenaar, J. J. *et al.* Sequencing of neuroblastoma identifies chromothripsis and defects in neuritogenesis genes. *Nature* **483,** 589–593 (2012).
25. Barone, G., Anderson, J., Pearson, A. D. J., Petrie, K. & Chesler, L. New strategies in neuroblastoma: therapeutic targeting of MYCN and ALK. *Clin. Cancer Res.* **19,** 5814–5421 (2013).
26. Maris, J. M. Recent advances in neuroblastoma. *N. Engl. J. Med.* **362,** 2202–2211 (2010).
27. Seeger, R. C. *et al.* Association of multiple copies of the N-*myc* oncogene with rapid progression of neuroblastomas. *N. Engl. J. Med.* **313,** 1111–1116 (1985).
28. Brodeur, G. M., Seeger, R. C., Schwab, M., Varmus, H. E. & Bishop, J. M. Amplification of N-myc in untreated human neuroblastomas correlates with advanced disease stage. *Science* **224,** 1121–1124 (1984).
29. Ala, U. *et al.* Integrated transcriptional and competitive endogenous RNA networks are cross-regulated in permissive molecular environments. *Proc. Natl Acad. Sci. USA* **110,** 7154–7159 (2013).
30. Denzler, R., Agarwal, V., Stefano, J., Bartel, D. P. & Stoffel, M. Assessing the ceRNA hypothesis with quantitative measurements of miRNA and target abundance. *Mol. Cell* **54,** 766–776 (2014).
31. Bosson, A. D., Zamudio, J. R. & Sharp, P. A. Endogenous miRNA and target concentrations determine susceptibility to potential ceRNA competition. *Mol. Cell* **56,** 347–359 (2014).
32. Agarwal, V., Bell, G. W., Nam, J.-W. & Bartel, D. P. Predicting effective microRNA target sites in mammalian mRNAs. *eLife* **4,** http://dx.doi.org/10.7554/eLife.05005 (2015).
33. Bartel, D. P. MicroRNAs: target recognition and regulatory functions. *Cell* **136,** 215–233 (2009).
34. Beckers, A. *et al.* MYCN-targeting miRNAs are predominantly downregulated during MYCN-driven neuroblastoma tumor formation. *Oncotarget* **6,** 5204–5216 (2015).
35. Maris, J. M. *et al.* Allelic deletion at chromosome bands 11q14-23 is common in neuroblastoma. *Med. Pediatr. Oncol.* **36,** 24–27 (2001).
36. Breen, C. J., O'Meara, A., McDermott, M., Mullarkey, M. & Stallings, R. L. Coordinate deletion of chromosome 3p and 11q in neuroblastoma detected by comparative genomic hybridization. *Cancer Genet. Cytogenet.* **120,** 44–49 (2000).
37. Ejeskär, K., Aburatani, H., Abrahamsson, J., Kogner, P. & Martinsson, T. Loss of heterozygosity of 3p markers in neuroblastoma tumours implicate a tumour-suppressor locus distal to the FHIT gene. *Br. J. Cancer* **77,** 1787–1791 (1998).
38. Bray, I. *et al.* Widespread dysregulation of MiRNAs by MYCN amplification and chromosomal imbalances in neuroblastoma: association of miRNA expression with survival. *PLoS ONE* **4,** e7850 (2009).
39. Chiang, H. R. *et al.* Mammalian microRNAs: experimental evaluation of novel and previously annotated genes. *Genes Dev.* **24,** 992–1009 (2010).
40. Roush, S. & Slack, F. J. The let-7 family of microRNAs. *Trends Cell Biol.* **18,** 505–516 (2008).
41. Hackett, C. S. *et al.* Genome-wide array CGH analysis of murine neuroblastoma reveals distinct genomic aberrations which parallel those in human tumors. *Cancer Res.* **63,** 5266–5273 (2003).
42. Karreth, F. A. *et al.* The BRAF pseudogene functions as a competitive endogenous RNA and induces lymphoma *in vivo*. *Cell* **161,** 319–332 (2015).
43. Maris, J. M., Hogarty, M. D., Bagatell, R. & Cohn, S. L. Neuroblastoma. *Lancet* **369,** 2106–2120 (2007).
44. Pugh, T. J. *et al.* Exome sequencing of pleuropulmonary blastoma reveals frequent biallelic loss of TP53 and two hits in DICER1 resulting in retention of 5p-derived miRNA hairpin loop sequences. *Oncogene* **33,** 5295–5302 (2014).
45. Rakheja, D. *et al.* Somatic mutations in *DROSHA* and *DICER1* impair microRNA biogenesis through distinct mechanisms in Wilms tumours. *Nature Commun.* **2,** 4802 (2014).
46. Iwakawa, R. *et al.* Genome-wide identification of genes with amplification and/or fusion in small cell lung cancer. *Genes Chromosom. Cancer* **52,** 802–816 (2013).
47. Thériault, B. L., Dimaras, H., Gallie, B. L. & Corson, T. W. The genomic landscape of retinoblastoma: a review. *Clin. Experiment. Ophthalmol.* **42,** 33–52 (2014).

Supplementary Information is available in the online version of the paper.

Acknowledgements G.Q.D. is supported by National Institutes of Health grant R01GM107536, Alex's Lemonade Stand Foundation, and the Ellison Medical Foundation. G.Q.D. is an affiliate member of the Broad Institute, and an investigator of the Howard Hughes Medical Institute and the Manton Center for Orphan Disease Research. J.T.P. was supported by Alex's Lemonade Stand Foundation. K.M.T. was supported as a Howard Hughes Medical Institute International Student Research Fellow and as a Herchel Smith Graduate Fellow. D.S.P. and R.E. were supported by award number T32GM007753 from the National Institute of General Medical Sciences.

Author Contributions G.Q.D. provided support and guidance for this work; G.Q.D. and J.T.P. conceived the hypothesis, designed the study, and wrote the manuscript; J.T.P. performed and interpreted most of the experiments and generated figures; K.M.T. helped perform the shRNA and siRNA experiments and generated most of the plasmid constructs; D.S.P. helped perform the RNA sequencing experiments; F.R., J.T., and F.B. generated the aCGH and survival data on neuroblastoma patients; C.S.S., K.C.K., and J.J.C. acquired tissue samples and assisted with the IHC analysis; R.E. assisted with the CRISPR experiments; M.S., Y.d.S., G.S.L.P., and S.J.R. provided technical help; P.C. processed RNA sequencing data and helped with data analysis; H.C.T. helped perform *in vitro* transfection experiments; A.H. assisted with RNA sequencing data analysis; J.K.O. and C.S.S. performed xenograft experiments; M.C. assisted with the RNA sequencing experiments.

Author Information Reprints and permissions information is available at www.nature.com/reprints. The authors declare competing financial interests: details are available in the online version of the paper. Readers are welcome to comment on the online version of the paper. Correspondence and requests for materials should be addressed to G.Q.D. (george.daley@childrens.harvard.edu).

METHODS

Cell culture. BE(2)C (ATCC CRL-2268), PA-1 (ATCC CRL-1572), IMR90 (ATCC CRL-186), SK-N-AS (ATCC CRL-2137), SH-SY5Y (ATCC CRL-2266), 293T(ATCC 11268), SK-N-DZ (ATCC CRL-2149), and Kelly cells (Sigma 92110411-1VL) were maintained in 1:1 DMEM/F12:MEM media with 10% inactivated fetal calf serum, 1 μg ml^{-1} penicillin, and 1 U ml^{-1} streptomycin. All cell lines were purchased for the purposes of this study, are not among commonly misidentified cell lines (according to the International Cell Line Authentication Committee), and tested negative for mycoplasma contamination.

Plasmids. *Turbo-RFP*, *LIN28B*, and *MYCN*(ORF) cDNAs were subcloned into the pcDNA3.1 expression vector (Invitrogen). The *MYCN* 3′ UTR was cloned from BE(2)C cDNA and subcloned into pcDNA3.1:*MYCN* to create pcDNA3.1:*MYCN*/3′ UTR. ShRNA-resistant-*LIN28B* and pcDNA3.1:*MYCN*/3′ UTR-*let-7*-site-mutant vectors were made using a QuikChange site-directed-mutagenesis kit (Stratagene) on pcDNA3.1:*LIN28B* and pcDNA3.1:*MYCN*/3′ UTR constructs, respectively. Wild-type and mutant *MYCN* 3′ UTRs were subcloned into pcDNA3.1:*RFP* and psiCHECK2 to create pcDNA3.1:*RFP*/*MYCN*-3′ UTRwt and pcDNA3.1:*RFP*/*MYCN*-3′ UTRmut as well as psiCHECK2:*MYCN*wt and psiCHECK2:*MYCN*mut. pIS1:*DICER*1, pIS1:*IGF2BP1*, and pIS1:*Hmga2* were gifts from D. Bartel[4,48] (Addgene plasmids 21649, 21639, and 14785). psiCHECK2-8x-let-7 was a gift from Y. Tomari[49] (Addgene plasmid 20931).

siRNA/*let-7* mimic transfections. BE(2)C and Kelly cells were reverse transfected using Lipofectamine 2000 (Life Technologies) into six-well plates using the appropriate siRNA or miRNA mimics (described below). Cells were harvested at time-points described for analysis by western blotting or qPCR. Growth assays were performed similarly, but in 96-well plates followed by time-point-specific BrdU growth assay. Global *let-7* target analysis was as follows: BE(2)C:*MYCN*-ORF cells co-transfected with control or *MYCN*-3′ UTR-2 siRNA and either control or *let-7a* miRNA mimic were harvested 48 h after transfection. Control siRNA (Life Technologies 439846). *LIN28B* siRNAs were as follows: ORF1 (Life Technologies 4392420, identifier s52479), ORF2 (Life Technologies 4392420, identifier s52477), 5′ UTR (GE Dharmacon Custom *LIN28B*-NM_001004317 Duplex siRNA, ON-TARGET Plus, sense: 5′-ACU GGA GAG AGG AGA GAA AUU-3′, antisense: 5′-UUU CUC UCC UCU CUC CAG UUU-3′), 3′ UTR-1 (GE Dharmacon J-028584-12-0020), 3′ UTR-2 (GE Dharmacon Custom *LIN28B*-NM_001004317 Duplex siRNA, ON-TARGET Plus, sense: 5′-CAA CAG UGA UUG UGA GAA UUU-3′, antisense: 5′-AUU CUC ACA AUC ACU GUU GUU-3′). *MYCN* siRNAs: ORF-1 (Life Technologies 4392420, identifier s9135), ORF-2 (Life Technologies 4392420, identifier s9134). Control miRNA mimic (Life Technologies 4464059), *let-7a* miRNA mimic (Life Technologies 4464066, identifier MC10050), *let-7a* inhibitor (Life Technologies 4464084, identifier MH10050).

Luciferase assays. For the *MYCN* 3′ UTR loss of function assays, BE(2)C cells were reverse co-transfected using Lipofectamine 2000 in quadruplicate into 96-well plates with the appropriate luciferase vector and either control siRNA, *MYCN* siRNA, or *let-7a* mimic. Sixty hours after transfection, luciferase activity was assayed using the Dual Luciferase Reporter Assay System (Promega). For the *MYCN* 3′ UTR gain of function assays, 293T cells were seeded into 96-well plates in quadruplicate and transfected using Lipofectamine 2000 the following day with the appropriate luciferase vector, *MYCN* 3′ UTR overexpression vector, and either control miRNA mimic or *let-7a* mimic. Luciferase activity was measured 24 h after transfection as described above.

Immunohistochemistry. Immunohistochemistry was performed on human tumour tissue sections as previously described[4] using anti-LIN28B antibody (Cell Signaling 4196) at a 1:400 dilution. Patient samples were obtained through Boston Children's Hospital IRB-CRS08-09-0429-2; Immunohistochemical and Molecular Analysis of Paediatric Tumours. Consent was obtained from all subjects.

Western blotting. Western blots were performed with antibodies against LIN28B (Cell Signaling 4196), LIN28A (Cell Signaling 3978), MYCN (Santa Cruz Biotechnology sc-53993), DICER1 Santa Cruz sc-30226), HK2 (Cell Signaling 2867S), IMP1 (Cell Signaling 2852S), tRFP (Origene TA150061), β-tubulin (Cell Signaling 2146), and β-actin (Santa Cruz Biotechnology sc-8342).

BrdU growth assay. Five thousand cells per well were plated on a 96-well plate in quadruplicate for each of three independent experiments. Cell proliferation was assayed relative to day 0 using a BrdU Cell Proliferation Assay Kit (Cell Signaling 6813) according to the manufacturer's protocol after incubation for 2 h with BrdU.

qPCR. Total RNA was isolated from cells using Trizol reagent (Life Technologies). For mRNA analysis, cDNA was prepared from 1 μg RNA using Superscript II Reverse Transcriptase (Life Technologies) and random hexamers. Twenty nanograms of cDNA was then used for qPCR with the SYBR Select Master Mix (Life Technologies). mRNA primers: *LIN28B* (forward: GAG TCA ATA CGG GTA ACA GGA C; reverse: CAC CAC AGT TGT AGC ATC TAT CT) *MYCN*-1 (forward: CGA TTC AGA TGA TGA AGA TGA TGA AG; reverse: GAC AGC CTT GGT GTT GGA), *IGF2BP1* (forward: CAG TCC AAG ATA GAC GTG CAT AG; reverse: CTC AGG GTT GTA AAG GGT AAG G), *DICER1* (forward: CTC CTA CCA CTA CAA TAC TAT CAC T; reverse: GGT CTT CAT AAA GGT GCT TGG T), *β-actin* (forward: GAC CCA GAT CAT GTT TGA GAC C; reverse: CGT AGC ACA GCT TCT CCT TAA T), *HMGA2* (forward: CTG CTC AGG AGG AAA CTG AAG; reverse: CAC TAA ACC TGG GAC TGT GAA G), *ARID3B* (forward: CAA GCA GAA TGG TGG TTT GG; reverse: ATG GAT GTG GGC AGG TTT AG). For *let-7* analysis, cDNA was prepared using 20 ng total RNA and a Taqman microRNA Reverse transcription kit (Life Technologies). Two nanograms of cDNA was then used for qPCR with the Taqman Universal PCR Master Mix (Life Technologies). Taqman microRNA Assays used (catalogue number 4427975): *let-7a* (identifier 000377), *let-7b* (identifier 002619), *let-7c* (identifier 000379) *let-7d* (identifier 002283), *let-7e* (identifier 002406), *let-7f* (identifier 000382), *let-7g* (identifier 002282), *let-7i* (identifier 002221), *miR-98* (identifier 000577), *U47* control microRNA Assay (identifier 001223). For both mRNA and *let-7* expression analysis, relative expression was determined using the ΔΔCT method, unless otherwise noted.

qPCR analysis of copies per cell. Total RNA per cell was determined by RNA harvest yield from 1.5×10^6 cells. For *MYCN* mRNA copies per cell, cDNA was prepared using 200 ng total RNA per cell type and from a dose curve of the synthetic *MYCN*-3′ UTR-RNA-fragment (Integrated DNA Technologies) with Superscript III Reverse Transcriptase (Life Technologies) and a *MYCN*-gene-specific primer (*MYCN*-2 rev). Ten per cent of the cDNA reactions were then used for qPCR as described above. Linear regression analysis was performed on *MYCN*-3′ UTR-RNA-fragment-sample CT values to determine the copies per reaction in the cell samples. *MYCN* mRNA copies per cell was then calculated on the basis of the total RNA per cell previously determined. Synthetic *MYCN*-3′ UTR-RNA-fragment sequence was as follows: 5′-TTC CTA GCC TGT TTC TTC CTG TTA ATG TAT TTG TTC ATG TTT GGT GCA TAG AAC TGG GTA AAT GCA AAG TTC TGT GTT TAA TTT CTT CAA AAT GTA TAT ATT TAG TGC TGC ATC TTA TAG CAC TT-3′. MYCN-2 qPCR primers: forward: CCT AGC CTG TTT CTT CCT GTT A; reverse: GTG CTA TAA GAT GCA GCA CTA AAT. A similar strategy was used to determine *let-7* copies per cell. Synthetic *let-7* RNA molecules for each *let-7* family member (Integrated DNA Technologies) were used in dose curves for cDNA reactions for each *let-7*. cDNA was prepared as described above, and 10% of cDNA reactions were used for qPCR as described above. Linear regression analysis of the synthetic-*let-7* qPCR cycle threshold values and total RNA per cell values were used to calculate copies per cell for each *let-7* family member.

RNA-seq analysis. We analysed copies per cell as follows. Sequence reads were aligned to the human transcriptome using HISAT version 0.1.6 (ref. 50). The transcriptome file used for polyA-RNA-based libraries consisted of protein-coding and ncRNA sequences downloaded from ENSEMBL (release 80) ftp://ftp.ensembl.org/pub/release-80/fasta/homo_sapiens/, as well as the ERCC control sequences. The transcriptome file used for short-RNA-based libraries consisted of mature microRNA sequences downloaded from mirBase (release 21: ftp://mirbase.org/pub/mirbase/), in addition to the synthetic short RNA spike in oligonucleotides (small RNA spikes: LET7A2-5′ SCR: /5Phos/rGrA rArGrA rUrGrU rGrGrU rGrUrU rGrUrA rUrArG rUrU; LET7I-5′ SCR: 5′-Phos-rGrG rUrArG rArUrA rGrUrU rGrUrG rCrUrG rUrU; MIR-NEG: 5′-Phos-rUrU rArCrG rUrCrG rUrCrG rCrGrU rCrGrU rUrArU rU; MIR17-5′ SCR: 5′-Phos-rArU rCrGrC rCrUrG rArUrA rArArG rUrGrC rArGrG rUrArG; JP_MIR-NEG DH1: 5′-Phos-rUrC rArCrA rArCrC rUrCrC rUrArG rArArA rGrArG rUrArG rA; JP_MIR-NEG DH2: 5′-Phos-rUrU rGrUrA rCrUrA rCrArC rArArA rArGrU rArCrU rG)[51]. To estimate transcript abundances, we applied Salmon version 0.3.2 (ref. 52) to the aligned reads and summarized transcript abundances into gene-level expression levels by summing all transcript expression levels mapping to the same gene. Gene-to-transcript mappings, and transcript type annotations, were downloaded also from ENSEMBL (ftp://ftp.ensembl.org/pub/release-80/gtf/homo_sapiens/). Unless otherwise stated, all RNA-seq data are presented as $\log_{10}(1 + \text{transcripts per million (TPM)})$, which we refer to as log(TPM) henceforth. To estimate the absolute copy number of transcripts per cell, we performed linear regression of the spike-in oligonucleotides concentration ($\log_{10}$) on the log(TPM) using the *lm* function in R for each sample. Using the slope and intercept estimated by this approach, we calculated the copies per cell of endogenous mRNA by determining the number of transcripts (on the basis of log(TPM) values) present in the total nanograms of RNA used for library preparation. We then determined molecules per cell on the basis of pre-determined picograms of RNA per cell. Global *let-7* target analysis was as follows: polyA-selected mRNA sequencing reads were processed as above, with no spike in RNAs used. RNA-seq data sets are available under GEO reference series GSE81500 (http://www.ncbi.nlm.nih.gov/geo/query/acc.cgi?acc=GSE81500).

Supplementary methodology: spike controlled quantification of small RNA. Through comparison with three miRNA spike-ins, including *let-7*-specific

5′-end-scrambled *let-7a* and *let-7i* spikes, we sought to minimize the effects of secondary structure bias known to exist during sRNA-seq library preparations, which can have significant effects on the relative efficiency of reads produced between different microRNAs[51] (Extended Data Fig. 6). A total of six synthetic spikes were used. Disparate reads per million observed among the equimolar small RNA spikes (that is, the miR-Neg, LET7A2, LET7I spikes have much higher read counts than equimolar MIR17, miRNegDH1, and miRNegDH2 spikes) demonstrate both the need to use spikes similar to the miRNA-of-interest to accurately determine copies per cell and the risk inherent in using a single spike to determine copies per cell for all miRNAs. The use of multiple miRNA-specific spikes improves upon previous miRNA quantification strategies using a single control miRNA to quantify all miRNAs[31] by limiting potential disparate read efficiencies between a single spike and the miRNA of interest. Difficulty in calculating relative expression of disparate miRNAs within a single data set because of such variable read efficiencies can therefore be mitigated through the use of spike-ins that closely resemble each miRNA of interest.

CRISPR/Cas9. Cas9/gRNA co-expressing lentiviral constructs (lentiCRISPRv2) were generated and lentiviral particles were produced as previously described[53,54], using protocols and gRNA design tools from http://www.genome-engineering.org. Puromycin selection began 24 h after lentiviral infection of BE(2)C and Kelly cells. Experiments were typically completed within 3 weeks of initial infection. Oligonucleotides used for gRNA cloning were as follows: *LIN28B* exon 2: CAC CGC ATC GAC TGG AAT ATC CAA G, AAA CCT TGG ATA TTC CAG TCG ATG C; *LIN28B* exon 3.1: CAC CGC AGA GCA AAC TAT TCA TGG A, AAA CTC CAT GAA TAG TTT GCT CTG C; *LIN28B* exon 3.2: CAC CGA ATG ATT ACC TAT CTC CCT T, AAA CAA GGG AGA TAG GTA ATC ATT C; *LIN28B* exon 4: CAC CGC CTT GTA GAT GCT ACA ACT G, AAA CCA GTT GTA GCA TCT ACA AGG C. Cas9/gRNA constructs: lentiCRISPRv2, lentiCRISPR:EGFPsgRNA-1, and lentiCRISPR:EGFPsgRNA-2 were gifts from F. Zhang[53,54] (Addgene plasmids 52961, 51760, and 51761).

shRNA. Lentiviral particles were prepared as previously described[11]. pLKO.1 short hairpin expression constructs (Sigma Mission shRNA): *LIN28B* shRNAs (sh1: TRCN0000144508, sequence 5′-CCTGTTTAGGAAGTGAAAGAA-3′; sh2: TRCN0000122599, sequence 5′-GCCTTGAGTCAATACGGGTAA-3′). Control vector (SHC001: no insert).

Xenografts. BE(2)C and SK-N-DZ cells were infected with either SHC001 or TRCN0000122599 pLKO.1 lentivirus, then puromycin selected for 48 h. One and a half million infected cells were injected subcutaneously into female Rag2 knockout (c57bl/6, 8-week-old) immune-deficient mice. Three weeks after injection, mice were killed and tumours were removed and weighed. This procedure was approved by the Boston Children's Hospital Institutional Animal Care and Use Committee under protocol 15-12-3071R, which limited xenograft tumour size to less than 2.0 cm.

aCGH analysis. Preparation of the 202 neuroblastoma aCGH data set has been previously described[55,56]. MicroRNA-containing loci were analysed for gain or loss as previously described[57]. Statistical significance between *MYCN*-amplified and non-amplified tumours was determined using a *t*-test with Welch's adjustment on original copy number values. Kaplan-Meyer curve generation and analysis was done using GraphPad Prism software.

ENCODE RNA-Seq data sets. Mature *let-7* expression data for 12 cell types were obtained from whole-cell small-RNA-Seq ENCODE/CSHL data sets, and *let-7* host transcript expression data from six cell types were obtained from RNA-seq ENCODE data sets on the University of California, Santa Cruz Genome Browser[58] (http://genome.ucsc.edu/). Expression levels were determined relative to *let-7c* and *let-7c* host transcript levels, respectively.

R2 database. Human neuroblastoma patient microarray and RNA-seq data sets were obtained from the R2: microarray analysis and visualization platform (http://r2.amc.nl) and analysed using GraphPad Prism software. Significance was determined by *t*-test with Welch's adjustment. Data sets used were Kozak (GEO accession number GSE45547) and SEQC (GEO accession number GSE62564).

Statistical analysis. No statistical methods were used to predetermine sample size. The experiments were not randomized. The investigators were not blinded to allocation during experiments and outcome assessment. Unless otherwise noted, all experiments were performed at least three times independently. Statistical tests used are identified in each figure legend. *P* values less than 0.05 were considered significant.

48. Mayr, C. & Bartel, D. P. Widespread shortening of 3′ UTRs by alternative cleavage and polyadenylation activates oncogenes in cancer cells. *Cell* **138,** 673–684 (2009).
49. Iwasaki, S., Kawamata, T. & Tomari, Y. *Drosophila* argonaute1 and argonaute2 employ distinct mechanisms for translational repression. *Mol. Cell* **34,** 58–67 (2009).
50. Kim, D., Langmead, B. & Salzberg, S. L. HISAT: a fast spliced aligner with low memory requirements. *Nature Methods* **12,** 357–360 (2015).
51. Hafner, M. *et al.* RNA-ligase-dependent biases in miRNA representation in deep-sequenced small RNA cDNA libraries. *RNA* **17,** 1697–1712 (2011).
52. Patro, R., Duggal, G. & Kingsford, C. Salmon: accurate, versatile and ultrafast quantification from RNA-seq data using lightweight-alignment. *bioRxiv* http://dx.doi.org/10.1101/021592 (2015).
53. Sanjana, N. E., Shalem, O. & Zhang, F. Improved vectors and genome-wide libraries for CRISPR screening. *Nature Methods* **11,** 783–784 (2014).
54. Shalem, O. *et al.* Genome-scale CRISPR-Cas9 knockout screening in human cells. *Science* **343,** 84–87 (2014).
55. Spitz, R. *et al.* Oligonucleotide array-based comparative genomic hybridization (aCGH) of 90 neuroblastomas reveals aberration patterns closely associated with relapse pattern and outcome. *Genes Chromosom. Cancer* **45,** 1130–1142 (2006).
56. Thiessen, J. *et al.* Chromosome 17/17q gain and unaltered profiles in high resolution array-CGH are prognostically informative in neuroblastoma. *Genes Chromosom. Cancer* **53,** 639–649 (2014).
57. Rushlow, D. E. *et al.* Characterisation of retinoblastomas without RB1 mutations: genomic, gene expression, and clinical studies. *Lancet Oncol.* **14,** 327–334 (2013).
58. Kent, W. J. *et al.* The human genome browser at UCSC. *Genome Res.* **12,** 996–1006 (2002).

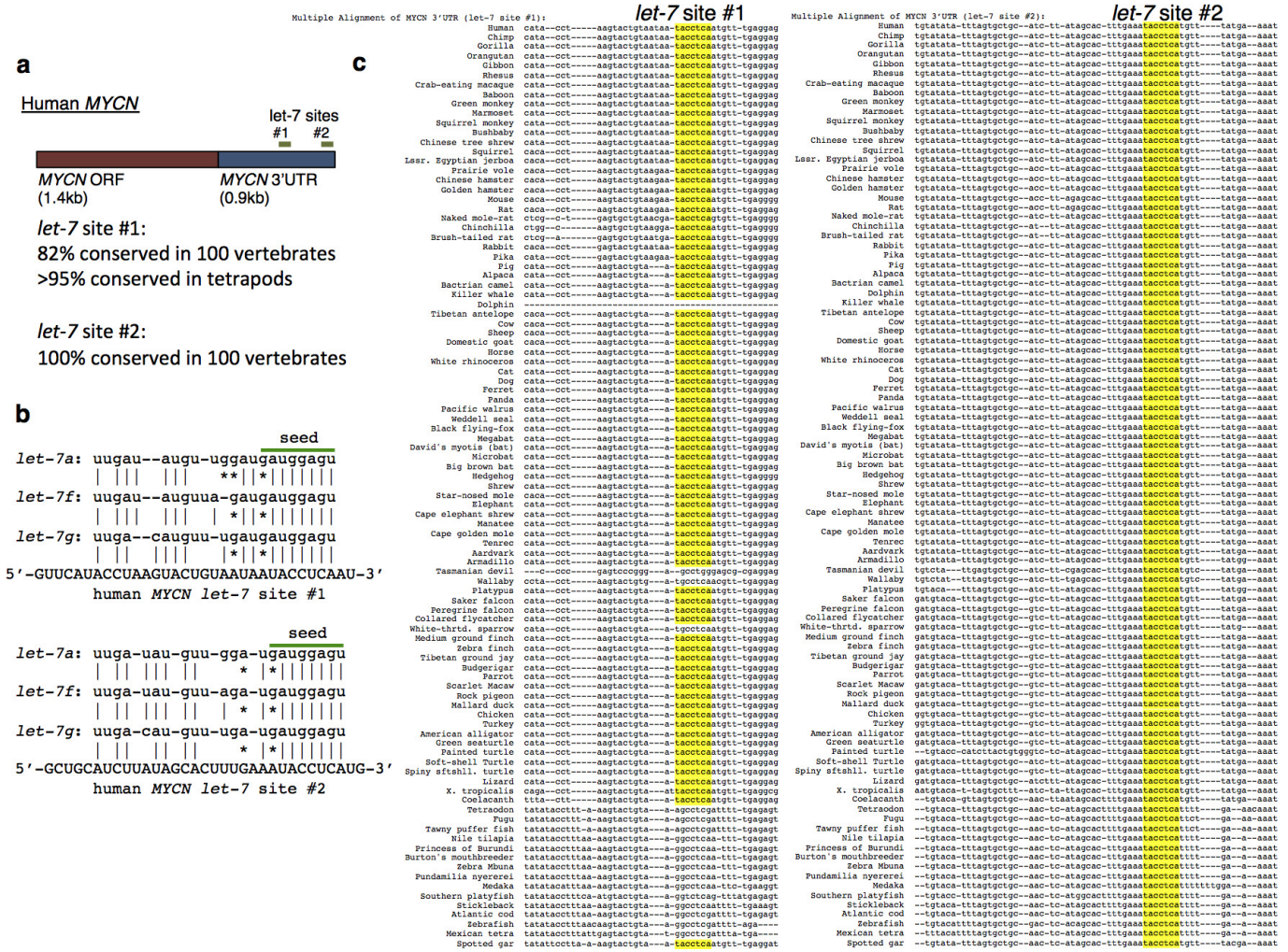

Extended Data Figure 1 | *MYCN* is a highly conserved *let-7* target. **a**, Schematic of human *MYCN* ORF and 3′ UTR, indicating *let-7* sites 1 and 2 and their approximate location. **b**, Predicted base pairing patterns of *let-7a*, *let-7f*, and *let-7g* with *MYCN let-7* sites 1 and 2. A–G base pairs, common in RNA, are represented by an asterisk. **c**, Alignments of *let-7* sites 1 and 2 in 100 vertebrate *MYCN* 3′ UTRs (ENCODE, https://genome.ucsc.edu/ENCODE/).

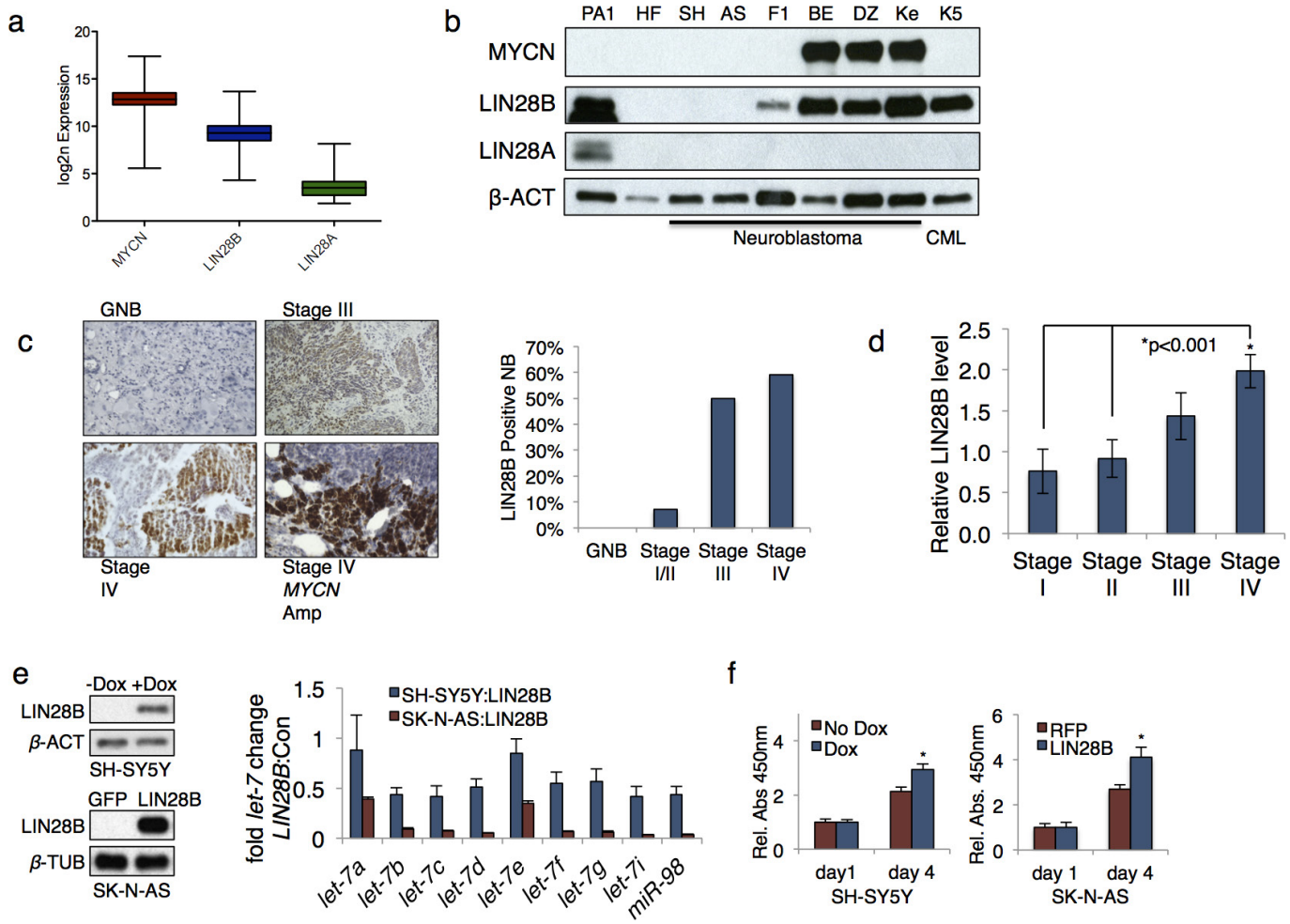

Extended Data Figure 2 | *LIN28B* expression and function in neuroblastoma. a, *MYCN*, *LIN28B*, and *LIN28A* mRNA expression levels in neuroblastoma ($n = 649$; see Source Data (ED Fig 2) in Supplementary Information). **b**, Immunoblot for indicated proteins in human embryonic carcinoma cells (PA1), normal human fibroblasts (HF), SK-N-SH (SH), SK-N-AS (AS), SK-N-F1 (F1), BE2C (BE), SK-N-DZ (DZ), Kelly (Ke), and human chronic myeloid leukaemia cells (K5). For gel source data, see Supplementary Figures. **c**, Representative LIN28B immunohistochemical staining of human neuroblastoma by stage (left), percentage LIN28B positive neuroblastoma by disease stage (right); ($n = 36$). GNB, ganglioneuroblastoma. **d**, *LIN28B* expression by neuroblastoma stage ($n = 64$; Source Data (ED Fig 2)). **e**, Immunoblot for LIN28B in inducible *LIN28B* SH-SY5Y cells and *GFP*- or *LIN28B*-expressing SK-N-AS cells (left) and corresponding qPCR analysis of relative *let-7* family levels (right) (mean plus s.e.m. of three independent experiments shown). **f**, Relative growth rate (BrdU incorporation, right) of SH-SY5Y and SK-N-AS neuroblastoma cells from **d** ($^*P < 0.05$, $n = 3$ independent experiments).

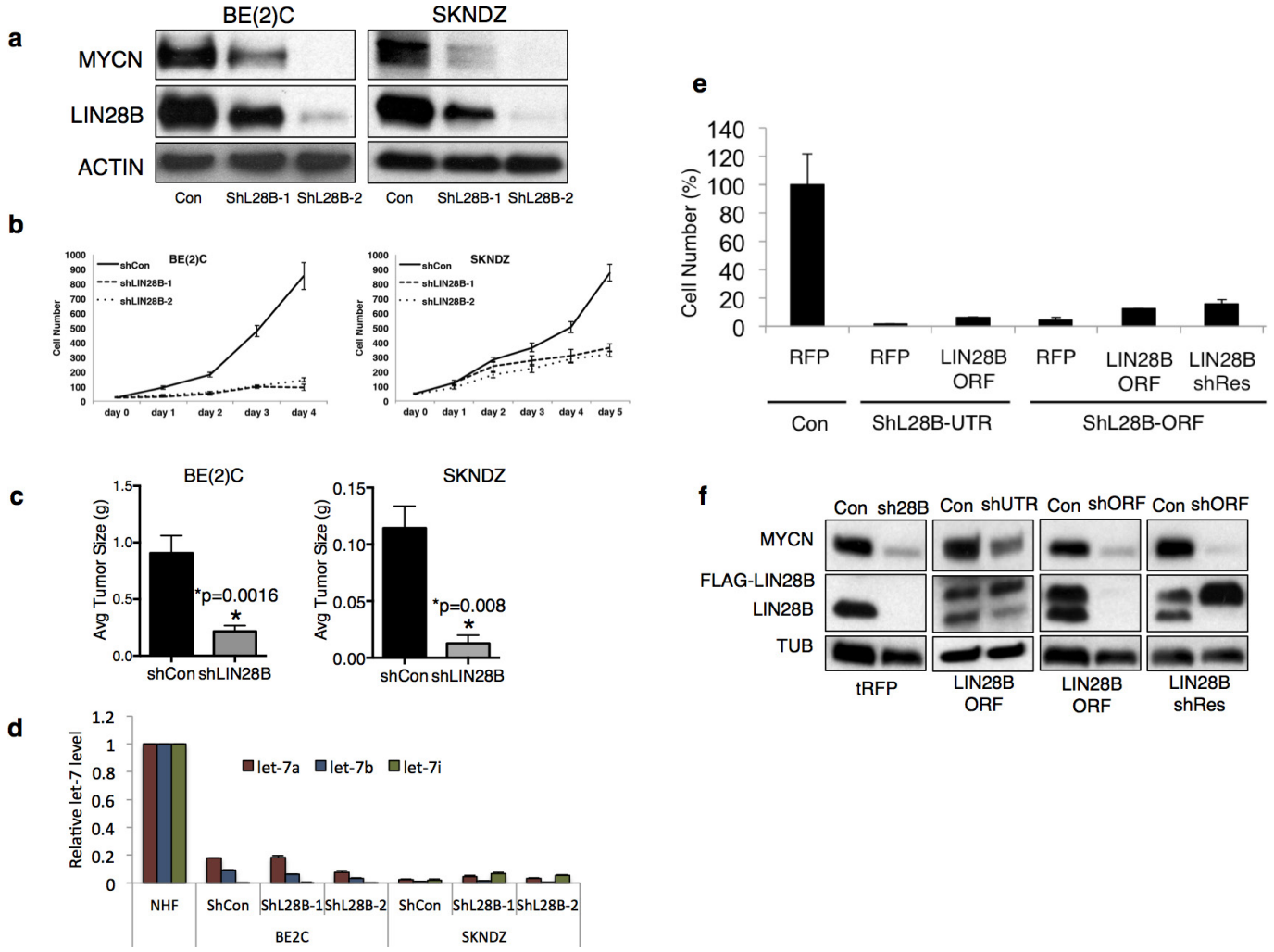

Extended Data Figure 3 | Short hairpin knockdown of *LIN28B* in neuroblastoma. a, Immunoblot for indicated proteins MYCN and LIN28B in *MYCN*-amplified cells infected with *LIN28B* targeting lentiviral shRNAs. For gel source data, see Supplementary Figures. **b**, Cell proliferation analysis of cells described in **a** ($n = 3$ independent experiments). **c**, Average tumour size of human–mouse subcutaneous xenograft tumour analysis 3 weeks after injection of 2×10^6 cells infected with a *LIN28B* targeting lentiviral shRNA ($n = 6$ mice for BE(2)C, $n = 3$ mice for SK-N-DZ; Supplementary Figures and Source Data (ED Fig 3)). **d**, qPCR analysis of *let-7a*, *let-7b*, and *let-7i* levels in cells described in **a** (mean plus s.e.m. of three independent experiments shown). **e**, Cell proliferation analysis of BE(2)C cells stably expressing red fluorescence protein (RFP), Flag-tagged *LIN28B* ORF, or shRNA resistant Flag-tagged *LIN28B* (LIN28B shRes) infected with *LIN28B* lentiviral shRNAs targeting the *LIN28B* 3′ UTR (ShL28B-UTR) or the *LIN28B* open-reading frame (ShL28B-ORF). Cell counts were performed 7 days after lentiviral shRNA infection (mean plus s.e.m. of three independent experiments shown). **f**, Immunoblot for indicated proteins in cells described in **e**. For gel source data, see Supplementary Figures.

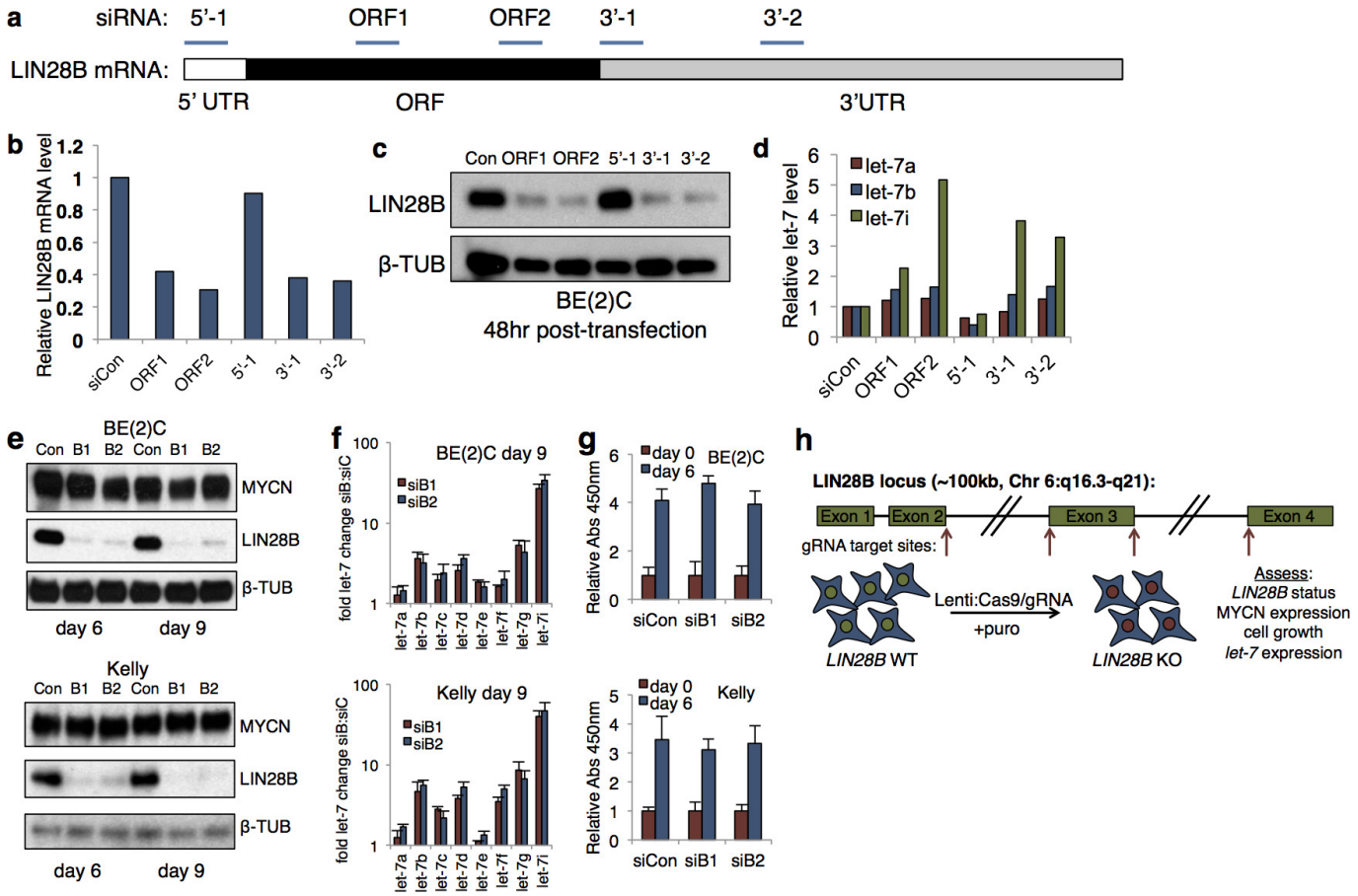

Extended Data Figure 4 | Small interfering RNA knockdown of *LIN28B* in neuroblastoma. a, Schematic of approximate siRNA target sites within the *LIN28B* mRNA. **b**, qPCR analysis of *LIN28B* mRNA levels in BE(2)C cells 48 h after transfection with the indicated *LIN28B* targeting siRNAs (mean of two independent experiments shown). **c**, Immunoblot analysis of LIN28B in cells from **a**. For gel source data, see Supplementary Figures. **d**, qPCR analysis of indicated *let-7* levels in cells from **a** (mean of two independent experiments shown). **e**, Immunoblot analysis of MYCN and LIN28B in serially transfected *MYCN*-amplified cells for 6 or 9 days. Identical transfections were performed on days 0, 3, and 6. For gel source data, see Supplementary Figures. **f**, Day 9 qPCR analysis of the *let-7* family in the cells from **a** ($n = 3$ independent experiments, mean plus s.e.m. shown). **g**, Cell growth analysis of day 0 to day 6 cells from **a** (BrdU incorporation, $n = 3$ independent experiments, mean plus s.e.m. shown). **h**, Lentiviral CRISPR-Cas9/*LIN28B* gRNA strategy targeting *LIN28B* at four distinct exon/intron junctions used in **b**–**g**.

a

% let-7 target site pool

let-7 target	BE(2)C	Kelly	SH-SY5Y
MYCN	19.24	18.52	0.15
DICER1	0.17	0.16	0.13
HK2	0.10	0.12	0.19
IMP1	0.96	2.97	0.07
LIN28B	0.66	0.70	0.14
ARID3B	0.29	0.60	0.35
HMGA2	0.10	0.11	0.09

b

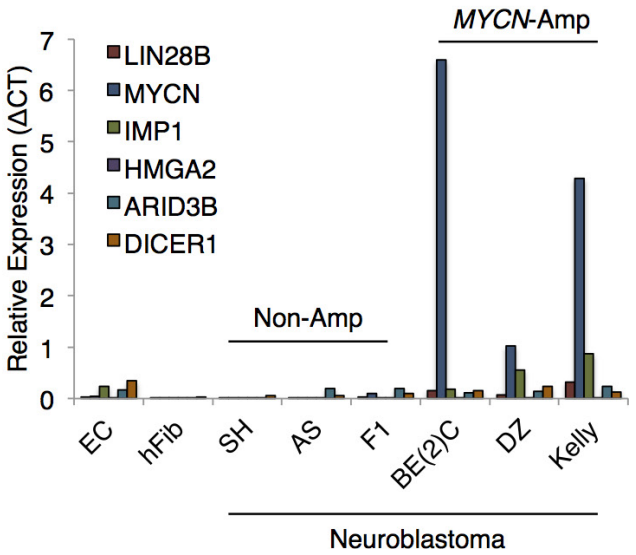

Extended Data Figure 5 | Relative levels of *let-7* targets in neuroblastoma. a, mRNA-seq *let-7* target table (as percentage *let-7* target-site pool). **b**, qPCR analysis of indicated *let-7* targets in neuroblastoma cells, PA1 embryonic carcinoma cells (EC), and normal human fibroblasts (hFib). Expression relative to *β-ACTIN* (ΔCT method) (mean of two biological replicates shown).

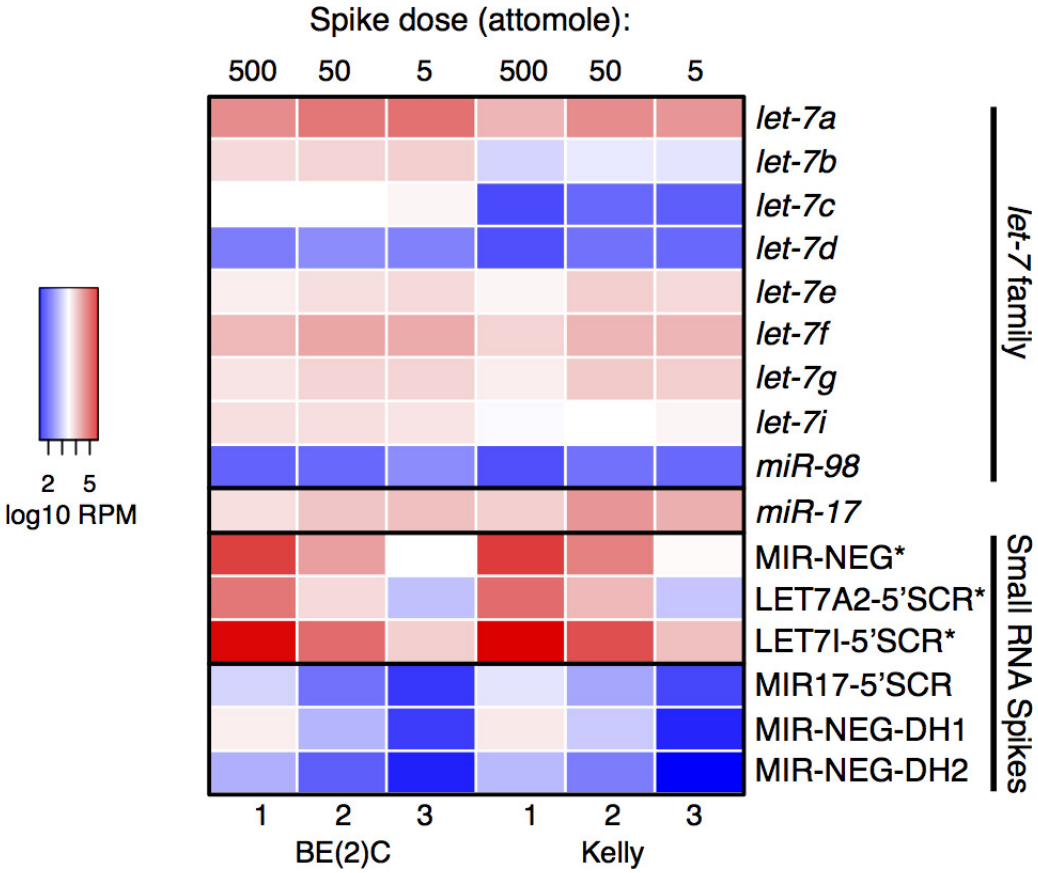

Extended Data Figure 6 | Heat map of *let-7* and small RNA spike reads. Heat map of three BE(2)C and three Kelly sRNA-seq samples depicting the relative reads per million of the *let-7* family, *miR-17*, and the six small RNA spikes added in equimolar amounts per sample (spikes miR-Neg, LET7A2, and LET7I were used to determine *let-7* copies per cell from the small RNA sequencing data set). RPM, reads per million.

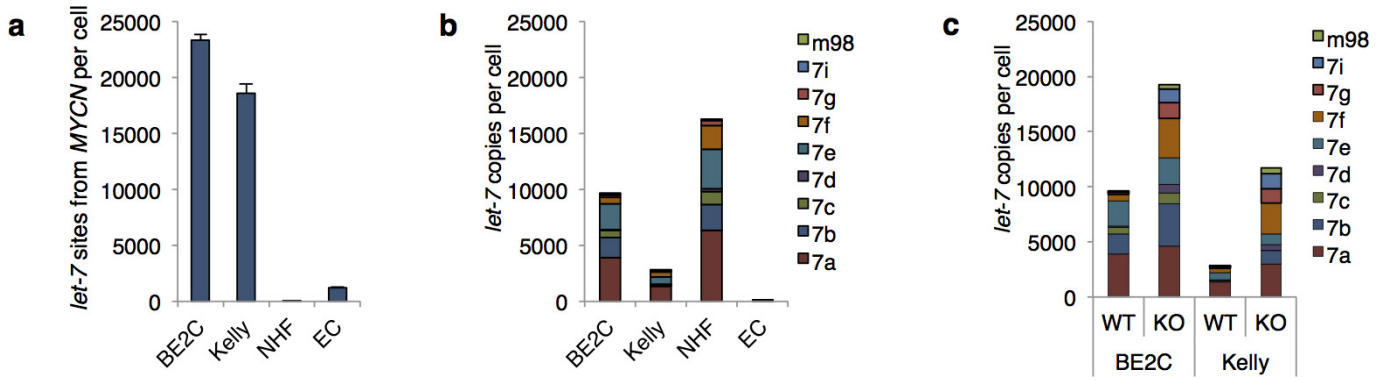

Extended Data Figure 7 | qPCR quantification of *MYCN* and *let-7* copies per cell. a, Total *let-7* sites per cell provided by *MYCN* mRNA in BE(2)C, Kelly, normal human fibroblasts (NHF), and embryonic carcinoma cells (EC) (mean plus s.e.m. of three biological replicates shown). **b**, Total *let-7* copies per cell in cells from **a**, presented as stacked graphs of all *let-7* family members (mean of three biological replicates shown). **c**, Total *let-7* copies per cell in wild-type or *LIN28B* knockout BE(2)C and Kelly cells, presented as stacked graphs of all *let-7* family members (values derived from *let-7* copies per cell in **b** and average *let-7* fold change described in Fig. 2f, g).

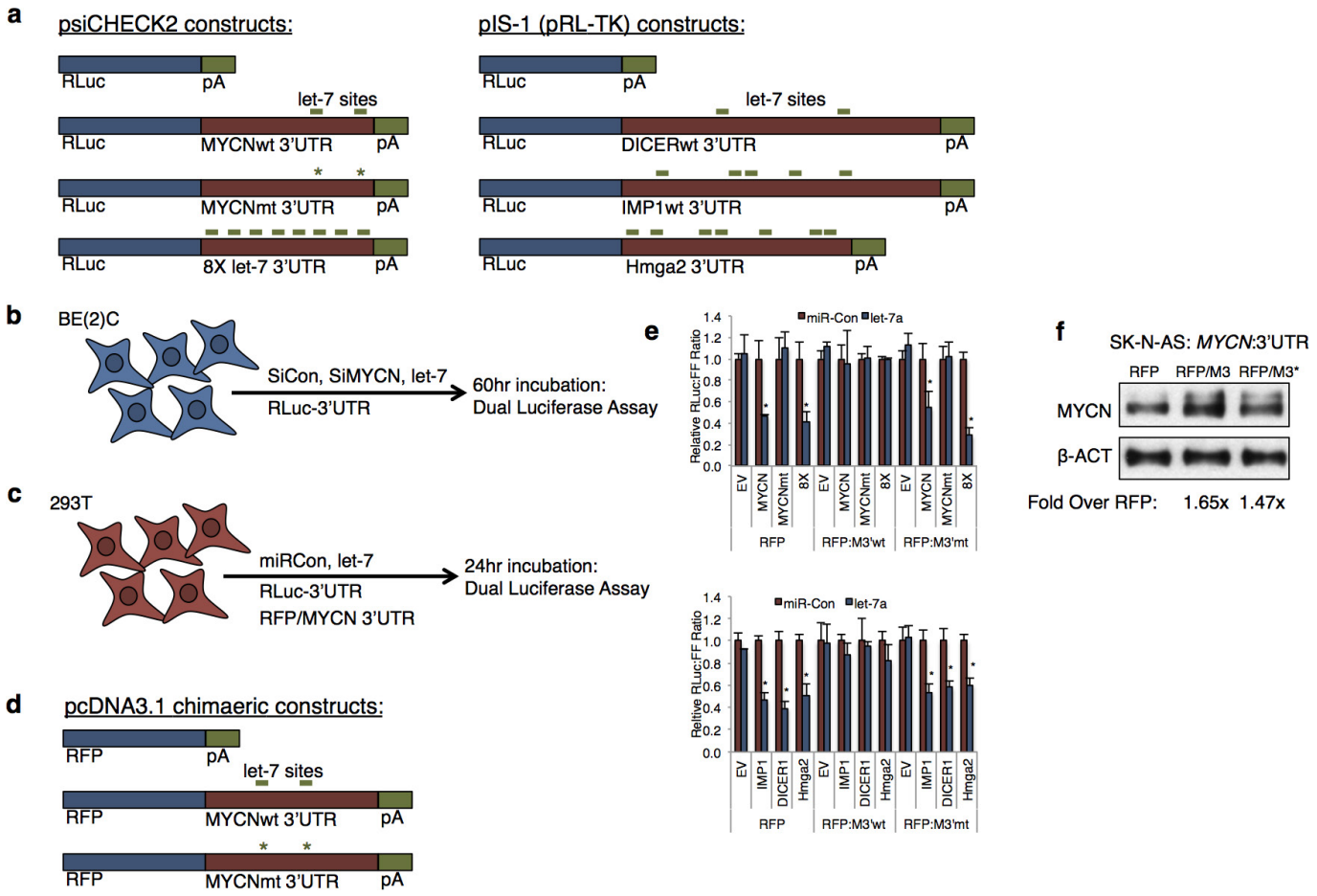

Extended Data Figure 8 | Luciferase reporter and gain of function constructs. a, Luciferase constructs used in the luciferase assays in Fig. 3d and Extended Data Fig. 8e. **b**, Schematic of the luciferase transfection protocols used in Fig. 3d. **c**, Schematic of the luciferase protocol used in Extended Data Fig. 8e. **d**, pcDNA3.1 constructs used in Extended Data Fig. 8e, f. **e**, Top: relative luciferase ratio in 293T cells co-transfected with the indicated 3′ UTR luciferase and pcDNA3.1 vectors in the presence of either control miRNA or *let-7a* mimic. Bottom: relative luciferase ratio in 293T cells co-transfected with the indicated 3′ UTR luciferase and pcDNA3.1 vectors in the presence of either a control miRNA or *let-7a* mimic. Mean of four independent experiments plus s.e.m. shown (*$P < 0.05$ relative to empty vector, unpaired *t*-test). **f**, Immunoblot analysis of MYCN in SK-N-AS cells stably expressing a *MYCN* ORF + 3′ UTR transgene and transfected with the indicated pcDNA3.1 vector. For gel source data, see Supplementary Figures.

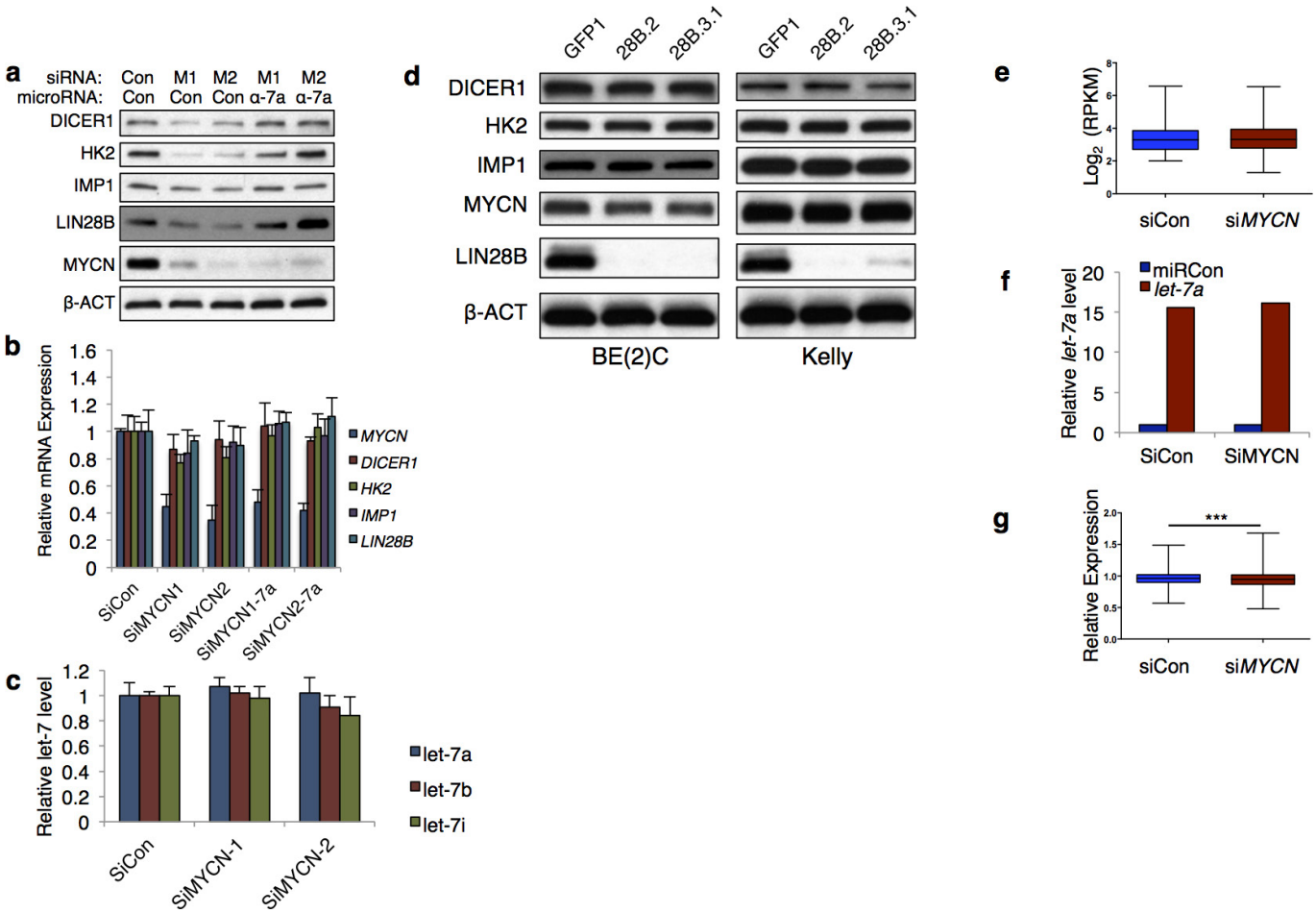

Extended Data Figure 9 | *MYCN* mRNA sponges *let-7*. **a**, Immunoblot analysis of indicated proteins in BE(2)C cells transfected for 2.5 days with control, *MYCN-1* (M1), or *MYCN-2* (M2) siRNA and either control microRNA or *let-7a* inhibitor. For gel source data, see Supplementary Figures. **b**, qPCR analysis of *DICER1*, *HK2*, *IMP1*, *LIN28B*, and *MYCN* in cells transfected as in **a**. **c**, qPCR analysis of *let-7a*, *let-7b*, and *let-7i* in BE(2)C cells transfected for 2.5 days with control siRNA, siM1, or siM2 ($n = 3$ independent experiments, mean plus s.e.m. shown). **d**, Immunoblot analysis of indicated proteins in cells infected with indicated Cas9-gRNA lentivirus. For gel source data, see Supplementary Figures. **e**, Expression levels of *let-7* targets in BE(2)C:*MYCN* cells transfected with siCon or si*MYCN*-3′ UTR. **f**, Relative *let-7* expression in BE(2)C:*MYCN* cells co-transfected with siCon or si*MYCN* (3′ UTR) siRNA and miRCon or *let-7a* mimic. A 16-fold increase in *let-7a* results in an approximately eightfold increase in total *let-7*, owing to *let-7a* making up almost half of the total cellular pool (Fig. 3c, lower). **g**, Relative expression levels of *let-7* targets in siCon and si*MYCN* cells transfected with *let-7a* mimic (data represent one round of mRNA-seq, $***P < 0.001$, one-tailed Wilcoxon test, GSE81497, see Source Data F3).

a % incidence in neuroblastoma patients

	3p21 loss	11q24 loss	3p/11q loss	MYCN Amp
Pugh, Morozova (n=240)	32.5	47.9	27.5	32.9
Spitz (n=90)	38.9	57.8		21.1
Maris (n=295)		42.0		31.8
Nair (n=86)	24.4	43.0	23.3	30.2

b Mature let-7 Level Analysis (sRNA Seq)

Name	Type	GEO Accession
IMR90	Lung Fibroblasts	GSM973680
HAoAF	Aortic Adventitial Fibroblats	GSM977035
HAoEC	Aortic Endothelial Cells	GSM977040
B-CD20+	B Cells	GSM977043
Mono-CD14+	Monocytes	GSM977044
HMSC-BM	Undifferentiated BM MSC	GSM977028
NHEK	Epidermal Keratinocytes	GSM897086
NHEM M2	Epidermal Melanocytes	GSM977047
HPC	Undifferentiated Pericytes	GSM977049
SKNSH	Non-Amp Neuroblastoma	GSM973667
HeLa	Cervical Cancer	GSM897079
MCF7	Breast Adenocarcinoma	GSM897081

c

let -7 locus	Host Transcript	Transcript Class	let-7 location
7a1, 7d, 7f1	LET7DHG	lncRNA	intron
7a2, miR100	MIR100HG	lncRNA	intron
7a3, 7b	LET7BHG	lncRNA	exon
7c, miR99a	MIR99AHG	lncRNA	intron
7e, miR99b	SPACA6P-AS	lncRNA	exon
7f2, miR98	HUWE1	protein coding	intron
7g	WDR82	protein coding	intron
7i	ENST00000550290	predicted lncRNA	intron

d Host-Transcript Expression Analysis (mRNA Seq)

Name	Type	UCSC Submission ID
NHLF	Lung Fibroblasts	3413
NHEK	Epidermal Keratinocytes	3473
HUVEC	Umbilical Vein Endothelial Cells	3470
HSMM	Skeletal Muscle Myoblasts	3468
H1-ESC	Embryonic Stem Cells	3464
HeLa	Cervical Carcinoma	3418

e

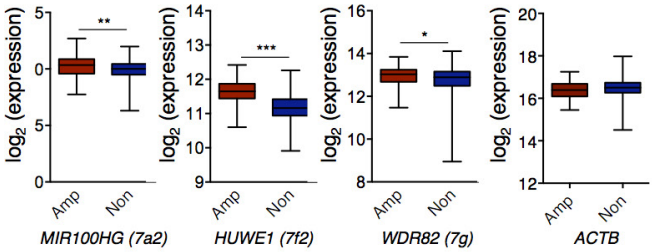

f

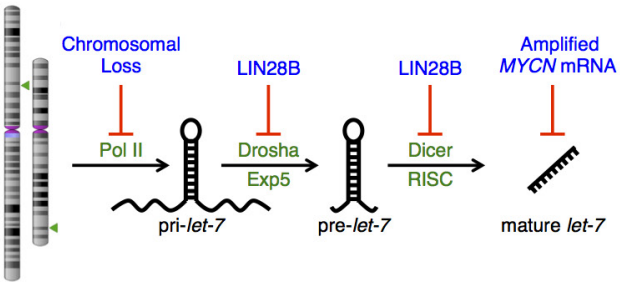

Extended Data Figure 10 | Neuroblastoma patient and ENCODE data. **a**, Detail of the incidence of chromosome 3p21 and 11q23 loss and *MYCN* amplification as determined by analysis of the indicated retrospective chromosomal aberration studies on neuroblastoma. **b**, List of the ENCODE sRNA-seq samples analysed (with associated GEO accession numbers) for the relative expression of mature *let-7* in Fig. 5c. **c**, List of *let-7* family host transcripts, transcript class, and *let-7* location within the transcript. **d**, List of the ENCODE mRNA-seq samples analysed (with associated University of California, Santa Cruz submission identifier numbers) for the relative expression of *let-7* host transcripts in Fig. 5d. **e**, Relative expression of *let-7a2*, *let-7f2*, and *let-7g* host genes by microarray in *MYCN*-amplified and non-amplified neuroblastoma. *ACTB* shown as control. $*P < 0.05$, $**P < 0.01$, $***P < 0.001$, unpaired *t-test*, $n = 643$, Source Data (ED Fig 10). **f**, Schematic showing the several mechanisms that impair *let-7* biogenesis and function in neuroblastoma (chromosome images created at http://www.ncbi.nlm.nih.gov/genome/tools/gdp/).